

Progress on Emerging Ferroelectric Materials for Energy Harvesting, Storage and Conversion

Xian-Kui Wei,* Neus Domingo, Young Sun, Nina Balke, Rafal E. Dunin-Borkowski, and Joachim Mayer

Since the discovery of Rochelle salt a century ago, ferroelectric materials have been investigated extensively due to their robust responses to electric, mechanical, thermal, magnetic, and optical fields. These features give rise to a series of ferroelectric-based modern device applications such as piezoelectric transducers, memories, infrared detectors, nonlinear optical devices, etc. On the way to broaden the material systems, for example, from three to two dimensions, new phenomena of topological polarity, improper ferroelectricity, magnetoelectric effects, and domain wall nanoelectronics bear the hope for next-generation electronic devices. In the meantime, ferroelectric research has been aggressively extended to more diverse applications such as solar cells, water splitting, and CO₂ reduction. In this review, the most recent research progress on newly emerging ferroelectric states and phenomena in insulators, ionic conductors, and metals are summarized, which have been used for energy storage, energy harvesting, and electrochemical energy conversion. Along with the intricate coupling between polarization, coordination, defect, and spin state, the exploration of transient ferroelectric behavior, ionic migration, polarization switching dynamics, and topological ferroelectricity, sets up the physical foundation ferroelectric energy research. Accordingly, the progress in understanding of ferroelectric physics is expected to provide insightful guidance on the design of advanced energy materials.


created his famous “sel polychreste.”^[2] The Rochelle salt is highly soluble in water and is very complex in crystal structure. About 160 years later, follow-up studies about pyroelectric, dielectric and piezoelectric properties finally establish the existence of ferroelectricity in Rochelle salt. After the finding of KH₂PO₄ in 1935,^[3] the first non-hydrogen-bonded FE BaTiO₃, with a simple perovskite structure, appears in the public vision in the early 1940s,^[4] which indicates that the spring of FE research comes. To date, more than 700 pure FE materials have been uncovered, including inorganic oxides, organic-inorganic hybrids, organic compounds and polymers, liquid crystals, and so on.^[5–7]

From the viewpoint of crystallography, an FE compound must adopt one of the ten polar point groups, that is, C₁, C_s, C₂, C_{2v}, C₃, C_{3v}, C₄, C_{4v}, C₆ and C_{6v}, out of the total 32 point groups.^[8] Considering the symmetry of all point groups, the belonging relationship classifies the dielectric materials, that is, ferroelectrics ⊆ pyroelectrics ⊆ piezoelectrics ⊆ dielectrics (Figure 1a). With the integration of pyroelectric, piezoelectric and dielectric properties, the ferroelectrics naturally secures a core position in the study of dielectrics.^[9–14] Benefitting from the robust responses to electric, mechanical, thermal, and optical fields, FE materials have been widely used in various modern electronic devices, such as varactors and memories,^[15,16] transducers and transistors,^[17] infrared detectors,^[18] microwave phase filters,^[19] piezoelectric microsensors and micromotors,^[20–22]

1. Introduction

It is well known that the study of ferroelectric (FE) materials starts from Rochelle salt, [KNaC₄H₄O₆]₃·4H₂O (potassium sodium tartrate tetrahydrate),^[1] which is the first compound discovered by Valasek in 1921. Looking back at history, we find that the time of exploring Rochelle salt may date back to 1665, when Seignette

X.-K. Wei, R. E. Dunin-Borkowski, J. Mayer
Ernst Ruska-Centre for Microscopy and Spectroscopy with Electrons
Forschungszentrum Jülich GmbH
52425 Jülich, Germany
E-mail: x.wei@fz-juelich.de

 The ORCID identification number(s) for the author(s) of this article can be found under <https://doi.org/10.1002/aenm.202201199>.

© 2022 The Authors. Advanced Energy Materials published by Wiley-VCH GmbH. This is an open access article under the terms of the Creative Commons Attribution-NonCommercial License, which permits use, distribution and reproduction in any medium, provided the original work is properly cited and is not used for commercial purposes.

DOI: 10.1002/aenm.202201199

N. Domingo
Catalan Institute of Nanoscience and Nanotechnology (ICN2)
CSIC and The Barcelona Institute of Science and Technology
Campus UAB, Bellaterra, Barcelona 08193, Spain

Y. Sun
Center of Quantum Materials and Devices and
Department of Applied Physics
Chongqing University
Chongqing 401331, China

N. Balke
Materials Science and Engineering
North Carolina State University
911 Partners Way, Raleigh, NC 27695, USA

J. Mayer
Central Facility for Electron Microscopy
RWTH Aachen University
Ahornstr. 55, 52074 Aachen, Germany

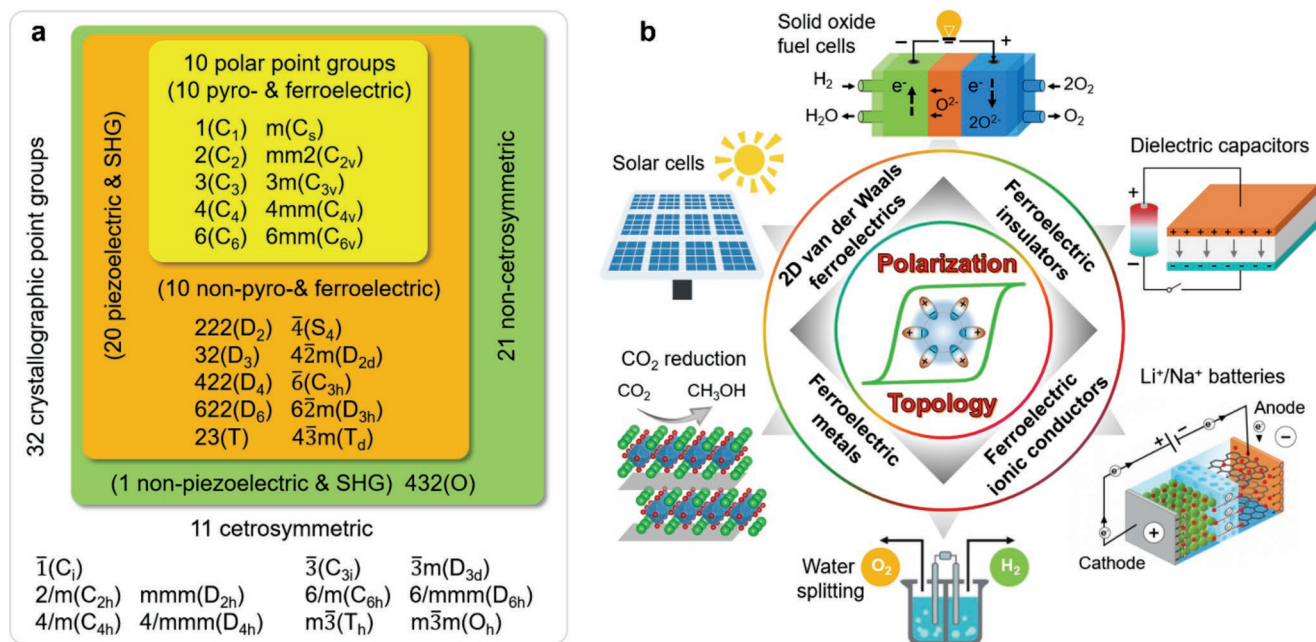


Figure 1. Expansion of ferroelectric phenomenon to energy materials. a) Belonging relationships of point groups and of ferroelectrics with pyroelectrics, piezoelectrics, and second-harmonic generation (SHG) based on the symmetry considerations. Reproduced with permission.^[8] Copyright 2012, American Chemical Society. b) Expansion of ferroelectric materials and their applications in various energy systems.

nonlinear optical devices,^[23] and capacitors.^[24] In the past decade, significant advances have been achieved in all aspects of material design and growth, structural characterization, theoretical calculation and property measurement. As underscored by the following findings, this thrived a new tide of FE research.

- I) By constructing delicate boundary conditions, for example, ultrathin dielectric-layer-based (PbTiO₃)_m/(SrTiO₃)_n superlattices,^[25] a number of emergent topological states such as polar vortices, polar skyrmions and dipole waves are discovered. Through breaking the restriction of polarization orientation confined by lattice symmetry, this promotes the FE research to the regime of intriguing topology.
- II) Many intriguing physical phenomena are observed at homogeneous and heterogeneous 2D boundaries of polar and nonpolar materials, for example, charged domain walls and SrTiO₃/LaAlO₃ interfaces. With involvement of polar catastrophe or discontinuity, interfacial 2D electron gas, magnetism, and superconductivity offer a great potential for design of miniaturized electronic devices.^[26–30]
- III) Other than insulators, FE metals characterized by coexisting ferroelectricity with metallicity emerge one after another. Alongside single-phase multiferroics, for example, FE ferromagnets or magnetic ferroelectrics,^[31,32] they provide a fertile platform for investigation of FE origin, interplay of polarity with intricate electronic and spin states^[33–35] as well as novel device applications.
- IV) Electrically switchable valley polarization^[36,37] and Moiré ferroelectricity^[38,39] reported in 2D layered van der Waals (vdW) materials delineate unsketched spaces for exploration of emerging FE physics at confined dimensions. The unprecedented electron-lattice-polarity correlation opens up a new era for study and design of low-dimensional electronic devices.^[40,41]

These findings highlight that entanglement of FE polarization with various electronic states is becoming more and more prominent in the newly emerging FE materials. With broadening of the material systems, another indisputable fact is that the FE research has been largely extended to energy-related applications (Figure 1b), for example, solar cells,^[42] electrostatic energy storage,^[43] water splitting,^[44,45] and CO₂ reduction.^[46] Motivated by urgent demand on clean and renewable energies, we therefore summarize the latest research progress about novel FE phenomena, their origin and correlation with enhanced performance in energy harvesting, storage and conversion. Instead of trying to be exhaustive in every direction, this review aims to offer fresh insights to comprehend the role of FE polarization in energy-related processes and activities. Based on mechanistic understanding, we believe that this review will help to attract more attention and inspire more research efforts in the fast-evolving joint fields of FE and energy materials.

2. Ferroelectric Origins and Phase Transitions

FE materials have a spontaneous polarization (P) that can be switched by an applied electric field (E), and breaking of spatial inversion symmetry—allowing unit-cell-wise separation of positive and negative charge centers—is a prerequisite condition for emergence of FE polarization. For an ordinary (or proper) FE, for example, BaTiO₃, Pb(Zr_{1-x}Ti_x)O₃ and BiFeO₃, the material undergoes a structural phase transition from a paraelectric phase to an FE phase at the Curie temperature T_C (Figure 2a). In compliance with lattice distortion, spontaneous polarization describes the symmetry change, thus the polarization vector is termed as a primary order parameter. Depending on symmetry of the lattices, the polarization direction can be fixed by

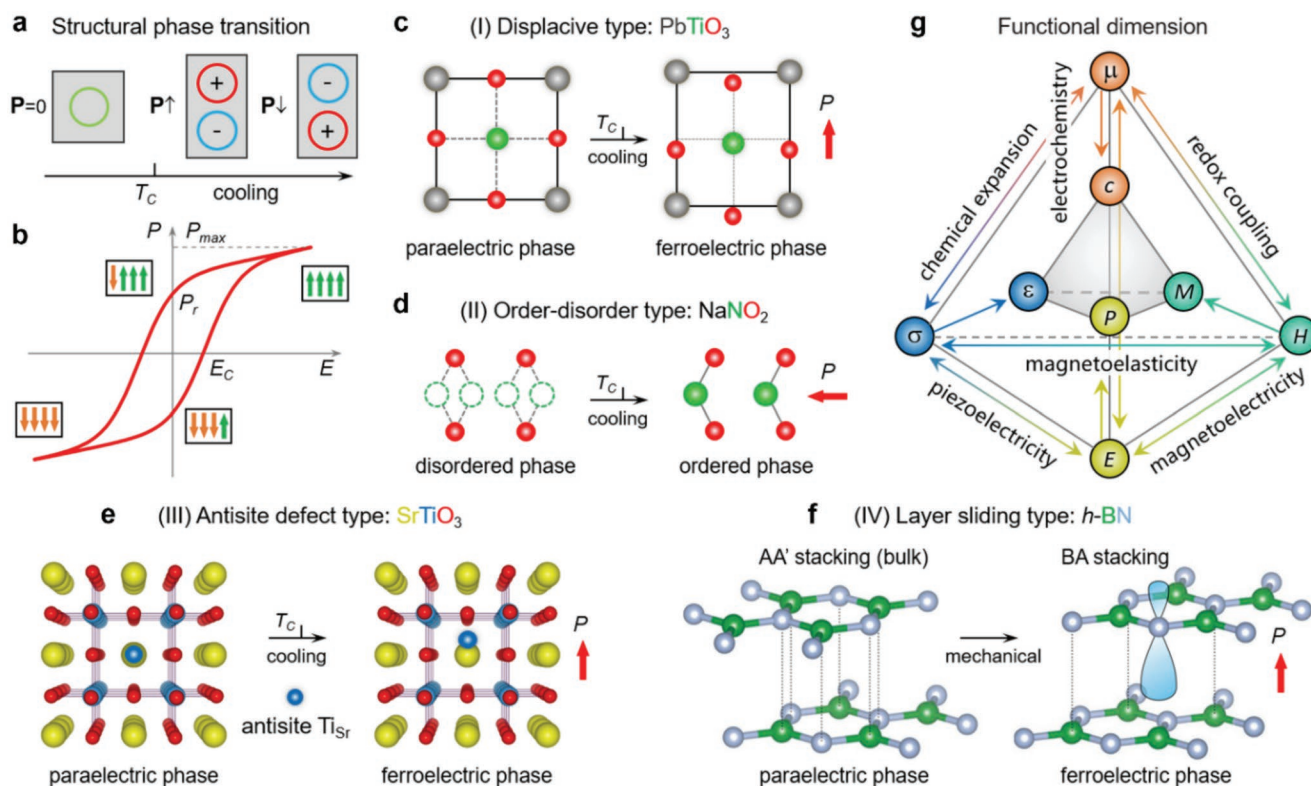


Figure 2. Ferroelectric phase transitions and multi-coupling functional dimension. a) Illustration of a paraelectric-to-ferroelectric phase transition via Curie temperature T_C . b) A typical P - E hysteresis loop of ferroelectrics and associating domain polarization reversal. c,d) Displacive and order-disorder type phase transitions as exemplified in PbTiO_3 and NbNO_2 , respectively. e,f) Creation of ferroelectricity by antisite defects and sliding layers as exemplified in SrTiO_3 and hexagonal BN (h -BN), respectively. Reproduced with permission.^[70] Copyright 2021, AAAS. g) An expanded functionality dimension of electric polarization (P) controlled by electric field (E) and their coupling with magnetism (M), strain (ϵ), concentration of ionic defects (c) alongside their conjugate fields of magnetic field (H), stress (σ) and chemical potential (μ). Reproduced with permission.^[76] Copyright 2013, AAAS.

a polar axis (e.g., tetragonal), a specific plane (monoclinic) or even without any constraint (triclinic).^[47–50] As a result of strain-polarization coupling, proper ferroelectrics exhibit large electromechanical and pyroelectric effects.^[9,51] If the polarization appears as a by-product of some other orders, for example, spin or charge, the ferroelectrics are called improper and the polarization is termed as a secondary order parameter. A number of single-phase multiferroic materials such as RMnO_3 (R = rare earth), LuFe_2O_4 and RMn_2O_5 belong to this category.^[31]

For a single-phase FE, a uniform polarization leads to net charging at sample surfaces due to uncompensated bound charges. To lower the electrostatic energy, the ferroelectrics tend to split into domains, which are separated by domain walls and differ in polarization orientation. Macroscopically, ferroelectrics are characteristic of a P - E hysteresis loop (Figure 2b), which results from switching of domain polarization and motion of domain walls.^[52] The maximum polarization (P_{max}), remnant polarization (P_r) and coercive field (E_c) manifest the FE property, and the loop area denotes the energy consumed in the polarization-switching event. So far, a general consensus is that there is no thickness limit on the existence of ferroelectricity,^[53–55] and the polarization may decouple with lattice tetragonality in perovskites at ultrathin conditions.^[56,57] At $T > T_C$, polar nanoclusters and precursor dynamics prevail in perovskite ferroelectrics below a temperature of $\approx T_C + 75$ K.^[58,59]

Among the FE oxides, it is noteworthy that materials like HfO_2 show an opposite thickness scaling behavior, whose FE property disappears above a critical thickness.^[60]

On the energy scale, to stabilize an FE state, a long-range electrostatic force should appear to compete with the short-range repulsive force, which usually favors a nonpolar symmetric structure.^[61] Corresponding to different origins and manifestations, the FE phase transitions can be classified into the following categories (Figure 2c–f). I) Displacive type phase transition. For instance in PbTiO_3 and BaTiO_3 , the Ti-3d and O 2p hybridization at $T < T_C$ plays an essential role in driving a collective off-center shift of Ti atoms away from centers of oxygen octahedra.^[62] II) Order-disorder type phase transition. Being sensitive to temperature change, the transition is a collapse process for atomic occupation from all possible sites to specific ones, for example, in NaNO_2 . In fact, these two types of phase transitions are not mutually exclusive but coexisting in many ferroelectrics.^[63,64] III) Antisite defect driven phase transition. Although with inhomogeneous distribution, atomic antisites such as Ti on Sr site (Ti_{Sr}) in SrTiO_3 ^[65,66] indeed give rise to emergence of robust ferroelectricity in originally nonpolar materials,^[32,67] which may possibly associate with off stoichiometry in composition. IV) Layer sliding driven phase transition. This adapts to stacking of homogeneous or heterogeneous 2D layered vdW materials.^[68–71] Taking hexagonal

BN (h-BN) as an example, a 180°-rotation between adjacent layers (AA' stacking) naturally restores the inversion symmetry broken in a monolayer. However, when BN monolayers slide into an AB or BA order, interlayer charge redistribution and associated ionic displacement result in an out-of-plane electric polarization.^[69,70] It is noteworthy that the FE origins are not limited to the above-mentioned situations, octahedral rotation mismatch at interfaces and vacancy-ordering-induced polyhedral distortion are other ways of generating ferroelectricity.^[72,73]

From the perspective of thermodynamic theory, the phase transitions can be classified into first-order and second-order transitions,^[74] which is manifested by discontinuity and continuity of derivatives of Gibbs free energy, for example, latent heat, volume change, and susceptibility, etc. Near a tricritical point, the first-order and second-order transitions can even compete and give rise to a frustrated-order transition, which leads to deviation from the classic mean-field theory and a number of anomalies in critical exponents and structure.^[75] These features indicate that the ferroelectric properties show great sensitivity to chemical composition, defect structure, boundary condition, and stimulus of external field. As a result, the ferroelectric polarization shows coupling to many other physical quantities and even their conjugate fields, for example, magnetism versus magnetic field (M vs H), strain versus stress (ϵ vs σ), defect concentration or conductivity versus chemical potential (c vs μ) and beyond (Figure 2g). Therefore, ferroelectrics offer a broad platform for exploration of intriguing physics and quite a few energy-related device applications.

3. Electrostatic Energy Storage Systems

3.1. Energy Storage Mechanism

An electrostatic capacitor consists of a dielectric insulator layer sandwiched by two parallel electrodes. Under application of an electric field (E), the stored capacitance (C) and recoverable energy density (U_e) can be expressed by

$$C = \epsilon_0 \epsilon_r A / d \quad (1)$$

$$U_e = \int_{P_r}^{P_{\max}} E dP \quad (2)$$

respectively (Figure 3a). Here, ϵ_0 , A , ϵ_r ($\gg 1$), d and dP are permittivity in vacuum ($\approx 8.85 \times 10^{-12}$ F m⁻¹), electrode overlapping area, relative permittivity, thickness and polarization increment of the dielectric layer. The electrostatic capacitors are capable of offering an ultrahigh power density (tens of MW kg⁻¹) at a time scale of ≈ 1 ms or less,^[77] ultrahigh energy efficiency ($\approx 97\%$),^[78] and ultrahigh operating voltage (up to MV cm⁻¹).^[79] Nowadays, dielectric capacitors are ubiquitously used in electronic devices and pulsed power systems, for example, hybrid electric vehicles, smart grids, avionic industries, high power lasers for military usage and consumer electronics.^[80] Specifically, antiferroelectric (AFE) and relaxor FE materials^[81,82] promise to deliver exceptional energy storage performance due to their reducible P_r and energy loss,^[83,84] improvable P_{\max} ^[85] and energy efficiency.^[78,86]

3.2. Novel Ferrielectric Phases in PbZrO₃-Based System

Nonpolar PbZrO₃ (space group Pbam), NaNbO₃ (Pbcm), and AgNbO₃ (Pbcm) are typical AFE materials,^[87-89] which undergo unit cell doubling from paraelectric cubic (C) phases to AFE orthorhombic (O) phases at T_C . For practical device usage, the AFEs are usually chemically modified to optimize its electrical and mechanical properties (Figure 3b), for example, doping of PbTiO₃ and PbSnO₃ into PbZrO₃ (termed as PZST). The aim is to lower its critical field (E_C) to an appropriate value below the dielectric breakdown strength (E_B).^[90,91] On the other hand, the energy levels of the FE phases, pertinent to vibrations of Pb ions and oxygen octahedral tiltings,^[92-94] can be tuned with respect to the AFE ground state to adjust the energy-storage performance (Figure 3c). Taking AFE PbZrO₃ as an example, its structure is dominated by antiparallel Pb displacements (≈ 24 pm) along a axis and antiferrodistortive (AFD) order of oxygen octahedra ($a^-a^-c^0$ in Glazer's notation), which rotate along $[210]_O$ and $[\bar{2}10]_O$ directions (Figure 3d). Compared with the ferroelectrics, concave curvatures of P - E hysteresis loops endow AFEs a natural advantage in effectively storing the electrostatic energy. Specifically, an inherent coupling of AFE-to-FE transition with the energy storage makes AFE materials ideal candidates for in situ biasing structural pathway studies.^[95-97]

Recently, intriguing improper ferroelectricity has been reported in PbZrO₃-based oxides. By taking illumination electron beam as an imaging source and a stimulus field, Wei et al. investigated time-dependent AFE-to-FE transitions using temporal- and atomic-resolution negative spherical-aberration (C_s) imaging (NCSI) technique in a transmission electron microscopy (TEM).^[98,99] During dynamic structural changes, a transient ferrielectric phase is discovered in $[001]_O$ -oriented PbZrO₃ between the AFE phase and FE monoclinic/rhombohedral phases. With preservation of antiparallel Pb displacements, ferrodistoritive (FD) distortion^[100] of oxygen octahedra gives rise to a cycloidal order of polarization in the ferrielectric phase (Figure 3e,f). In ABO₃ perovskites, a steric linkage of BO₆ framework usually constrains octahedral rotations to have equal magnitudes but opposite sense in a plane, thereby preserving inversion symmetry. Analogous to interfacial patterning of octahedral distortion,^[72,101,102] an AFD-to-FD phase transition points out a new improper approach^[103] to transform nonpolar materials into polar ones and realize ferroelectricity with non-collinear polarization features.

Associated with dilute La or Nb replacement at A site, Sn and Ti doping at B site of PbZrO₃ leads to incommensurate modulations (ICMs),^[104,105] which are manifested by $\frac{1}{n}\{110\}_C$ (n is a non-integer between 4 and 10) superstructure reflection in reciprocal space. In real space, the ICMs result from a mixture of stripes, whose thickness stochastically ranges from two to six layers of the $(110)_C$ plane. Previously, the Pb displacements are assumed to arrange in a fully compensated antiparallel fashion. However, by combining atomic-scale scanning TEM (STEM) analysis and density functional theory (DFT) calculations, Ma et al. found that the Pb displacements in Nb-doped PZST^[106,107] are either antiparallel with different magnitudes, or nearly orthogonal between adjacent stripes (Figure 3g,h). The imbalanced cationic displacements evidence the presence

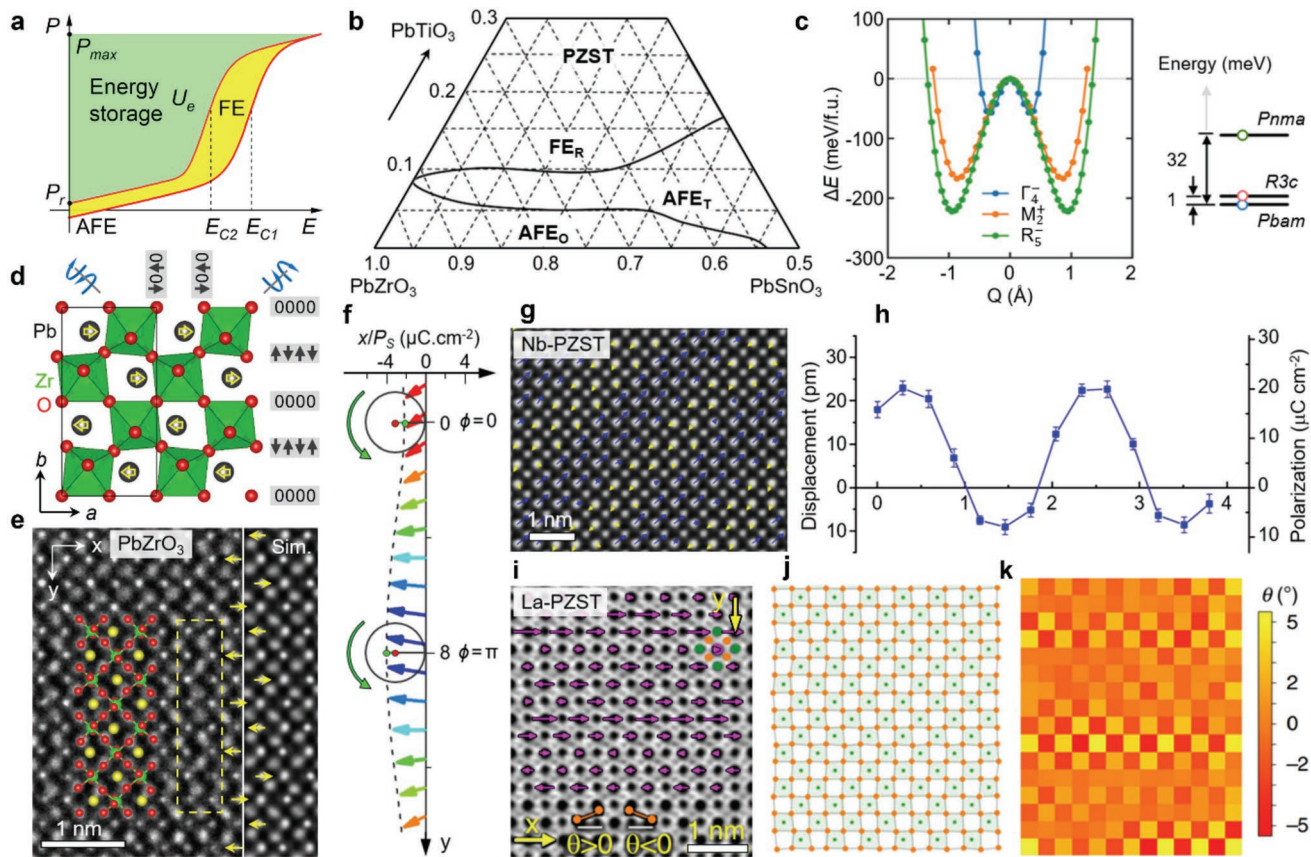


Figure 3. Wavy polarization orders in PbZrO_3 -based system. a) Half hysteresis loop of AFEs at $E \geq 0$ with annotation of E_{C1} , E_{C2} , P_{max} , P_r and energy storage density U_e (green area). b) Ternary phase diagram of PbZrO_3 - PbTiO_3 - PbSnO_3 (PZT). Reproduced with permission.^[10] Copyright 1964, Elsevier. c) Calculated potential energy of unstable high-symmetry phonon modes (Γ -point FE distortion, M-point in-phase tilting, and R-point out-of-phase tilting) and energy levels of stable PbZrO_3 phases. Reproduced with permission.^[94] Copyright 2019, American Physical Society. d) Structural model of AFE PbZrO_3 . e) NCSI-TEM images and refined structural model (Pb-yellow, Zr-green, O-pink circles) for the ferrodistortive (FD) phase of PbZrO_3 induced by electron beam irradiation along $[001]_O$ direction. Yellow arrows—antiparallel Pb shifts, yellow rectangle—FD unit cell. f) 2D cycloidal polarization order of the FD phase of PbZrO_3 .^[98] g, h) High-angle annular-dark field (HAADF) STEM image overlaid by Pb displacements and polarization profile of $[001]_C$ -oriented $(\text{Pb}_{0.99}\text{Nb}_{0.02})[(\text{Zr}_{0.57}\text{Sn}_{0.43})_{1-y}\text{Ti}_y]_{0.98}\text{O}_3$ (PZ-100y, $y = 0.05$). Reproduced with permission.^[106] Copyright 2019, American Physical Society. i–k) ABF-STEM image overlaid by Pb- $[100]_O$ displacements, tilting and distortion map of BO_6 octahedra and y-direction rippling map of O sublattices in $[001]_C$ -oriented $\text{Pb}_{0.97}\text{La}_{0.02}(\text{Zr}_{0.50}\text{Sn}_x\text{Ti}_{0.50-x})\text{O}_3$ (PLZST 50/45/5), respectively. Reproduced according to the terms of the CC-BY license.^[108] Copyright 2020, The authors, published by Springer Nature.

of ferroelectricity along the $[110]_C$ direction. By imaging oxygen atoms using annular-bright field (ABF) technique,^[108] Fu et al. further unveiled coupling of cationic shift with oxygen displacement along y direction in La-doped PZST (Figure 3i–k). Being consistent with results of synchrotron X-ray and neutron diffraction,^[109] the wavy polarization orders interpret origin of linear polarization response and non-zero P_r in the P - E loop of PbZrO_3 -based systems.^[99] Given the group-subgroup relationship between FD and FE phase transitions,^[74] the findings broaden the avenue of seeking for candidate energy-storage systems through chemical, defect, and strain engineering.^[72,85]

3.3. Nonpolar-to-Polar Transition in SrTiO_3 -Based System

SrTiO_3 has a cubic structure (space group $\text{Pm}\bar{3}\text{m}$) at room temperature. With lowering of temperature to $T < T_C = 105$ K, it transforms to a tetragonal phase (I4/mcm), which is featured by antiphase rotation of TiO_6 octahedra along c axis ($a^0a^0c^-$ in

Glazer's notation).^[111] At the mesoscopic scale, this leads to formation of inherent ferroelastic domains. Despite being nonpolar, SrTiO_3 receives enduring attention because of its abundant usage as substrate materials. In parallel, it also possesses many fascinating physical properties such as spin-charge conversion,^[112] superconductivity,^[113] magnetism and polarity at ferroelastic domain walls.^[29,114] By combing through the literature, one can see that these fascinating properties correlate intimately with one "hidden" physical quantity—FE polarization. In fact, its ferroelectricity ($P_{max} = 1.5 \mu\text{C cm}^{-2}$) has been proved by Weaver in 1959 below $T_q \approx 45$ K,^[115] which is a classic-to-quantum paraelectric transition temperature. Nowadays, it has been established that through strain engineering,^[116,117] its FE T_C can be increased to room temperature (Figure 4a). Other than that, it is reported that excitation of optical pump and terahertz electric field can also stabilize its metastable ferroelectricity, with T_C up to ≈ 290 K.^[118,119]

As for the abnormal ferroelectricity below T_q , one opinion argues that it arises from FE antiphase boundary, which is

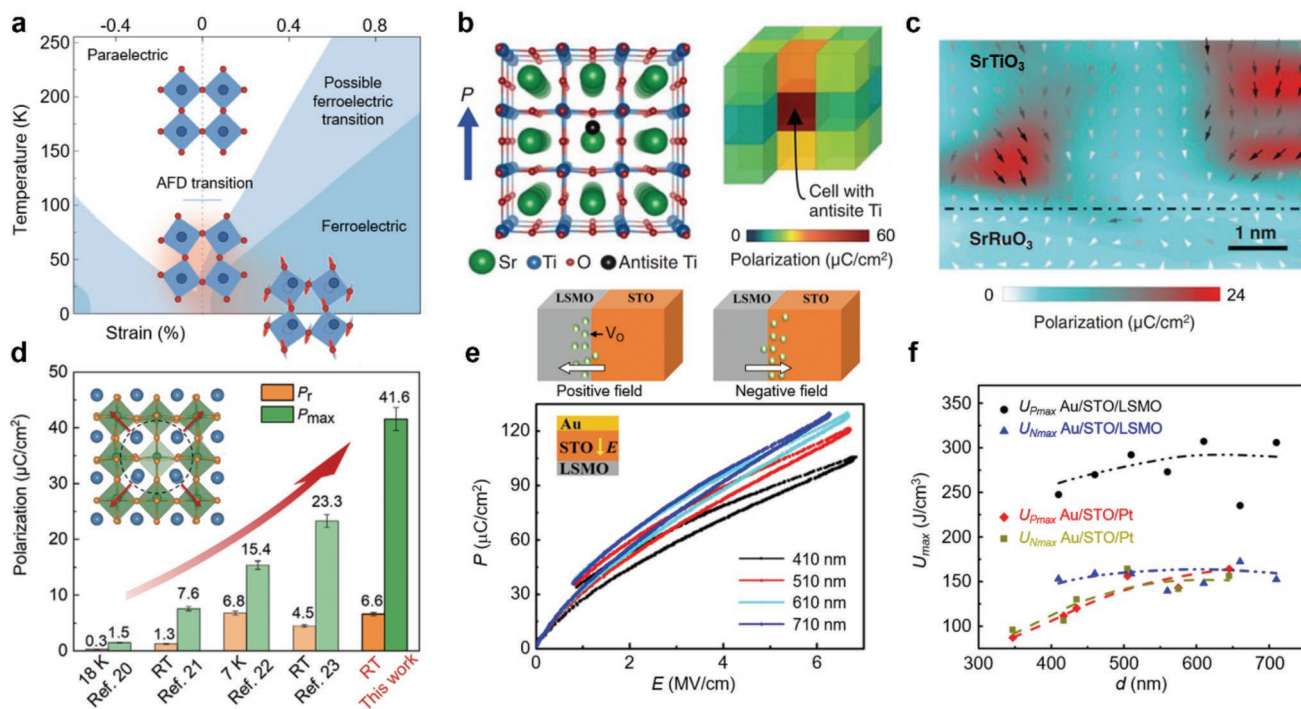


Figure 4. Ferroelectric origins and energy storage in SrTiO₃-based system. a) Temperature-strain phase diagram of SrTiO₃ (STO) pertinent to an AFD transition and then further to a ferroelectric phase. Reproduced with permission.^[118] Copyright 2019, AAAS. b,c) Antisite Ti_{Sr} atom induced polarization along the [001] direction, local 3D polarization profile obtained from the DFT calculations and polarization vector map estimated from atomic displacements in the ABF-STEM image. Reproduced with permission.^[65] Copyright 2015, AAAS. d) Comparison of remnant polarization (P_r) and maximum polarization (P_{max}) between Ti/O-deficient SrTiO₃ and the data from literature cited therein. The inset is the calculated unit cell of Ti/O-deficient SrTiO₃. Reproduced with permission.^[85] Copyright 2021, Wiley-VCH. e,f) P - E loops of Au/STO/(La_{0.67}Sr_{0.33})MnO₃ (LSMO) capacitors under positive field and energy density of Au/STO/LSMO and Au/STO/Pt capacitors under positive and negative fields (U_{Pmax} , U_{Nmax}) as a function of film thickness at room temperature. Reproduced with permission.^[79] Copyright 2017, American Chemical Society.

supported by results of Landau theory, first principles calculations and low-temperature scanning stress microscopy.^[114,120,121] Another opinion argues that the ferroelectricity is associated with an order-disorder transition,^[122,123] which relates to the emergence of polar rhombohedral clusters from a nonpolar tetragonal matrix below ≈ 70 K. Thus, the role of strain is to establish long-range correlation of preexisting polar nanoclusters. Specifically, Jang et al. pointed out that the polar nanoclusters likely originate from minute amounts of Sr deficiency.^[124] Using first-principles calculations and ABF-STEM characterization, Lee et al. demonstrated that structural defects with a form of atomic antisite,^[66,65] that is, Ti on Sr site (Ti_{Sr}) or vice versa, can give rise to a stable room-temperature ferroelectricity in SrTiO₃ even at reduced dimension (Figure 4b,c). Through introducing Ti/O vacancies, Li et al. further showed that defect-induced nanoregions can trigger an ultrahigh T_C ,^[85] which is up to ≈ 1098 K for the cubic-to-tetragonal transition. At room temperature, the tetragonal phase has a very large tetragonality value ($c/a = 1.038$) and the maximum polarization is up to $P_{max} = 41.6 \mu\text{C cm}^{-2}$ (Figure 4d). Yet, its P_r value is only $6.6 \mu\text{C cm}^{-2}$ owing to the relaxor nature of the polar clusters.

These unique features indicate that defect-engineered SrTiO₃ are very suitable for electrostatic energy storage. In Au/SrTiO₃/La_{0.67}Sr_{0.33}MnO₃ (LSMO) multilayers,^[79] Hou et al. found that the P_{max} can astonishingly rise to $\approx 120 \mu\text{C cm}^{-2}$ at $E = 6.8 \text{ MV cm}^{-1}$ (Figure 4e). Under positive and negative

E , the recoverable energy density swaps between 300 and 150 J cm^{-3} (energy efficiency $\eta > 85\%$), which are the highest values reported so far.^[82,125] When the bottom electrode LSMO is changed to Pt, a stable U_e with values around 150 J cm^{-3} can still be obtained (Figure 4f). In combination with atomic-scale STEM study, Hou et al. argued that inter-diffusion of oxygen vacancies (V_O) and electric field modulation near the SrTiO₃/LSMO interfaces are responsible for the exceptional storage performance. However, a dramatic thickness difference, interface (≈ 5 nm) versus SrTiO₃ film (410–710 nm), questions the decisive role of the interface only. On the contrary, associated with a metal-to-insulator transition of the LSMO electrode, that is, perovskite-to-brownmillerite phase transformation,^[126,127] electrochemical activities relating to migration of vacancies and cations via antisite defects and change of elemental valence states, seem to play an important role in the energy storage and release processes.

3.4. Na_{0.5}Bi_{0.5}TiO₃-Based Ferroelectric Ionic Conductors

Considering the harm of Pb to the environment and human health, lead-free ferroelectrics^[128,129] such as BaTiO₃ and (K_{1-x}Na_x)NbO₃ are widely investigated to replace Pb-based ones. Because of having exceptional piezoelectricity and pyroelectricity, relaxor FE Na_{0.5}Bi_{0.5}TiO₃ (NBT, $E_g = 3.1 \text{ eV}$)^[130] serves as an important

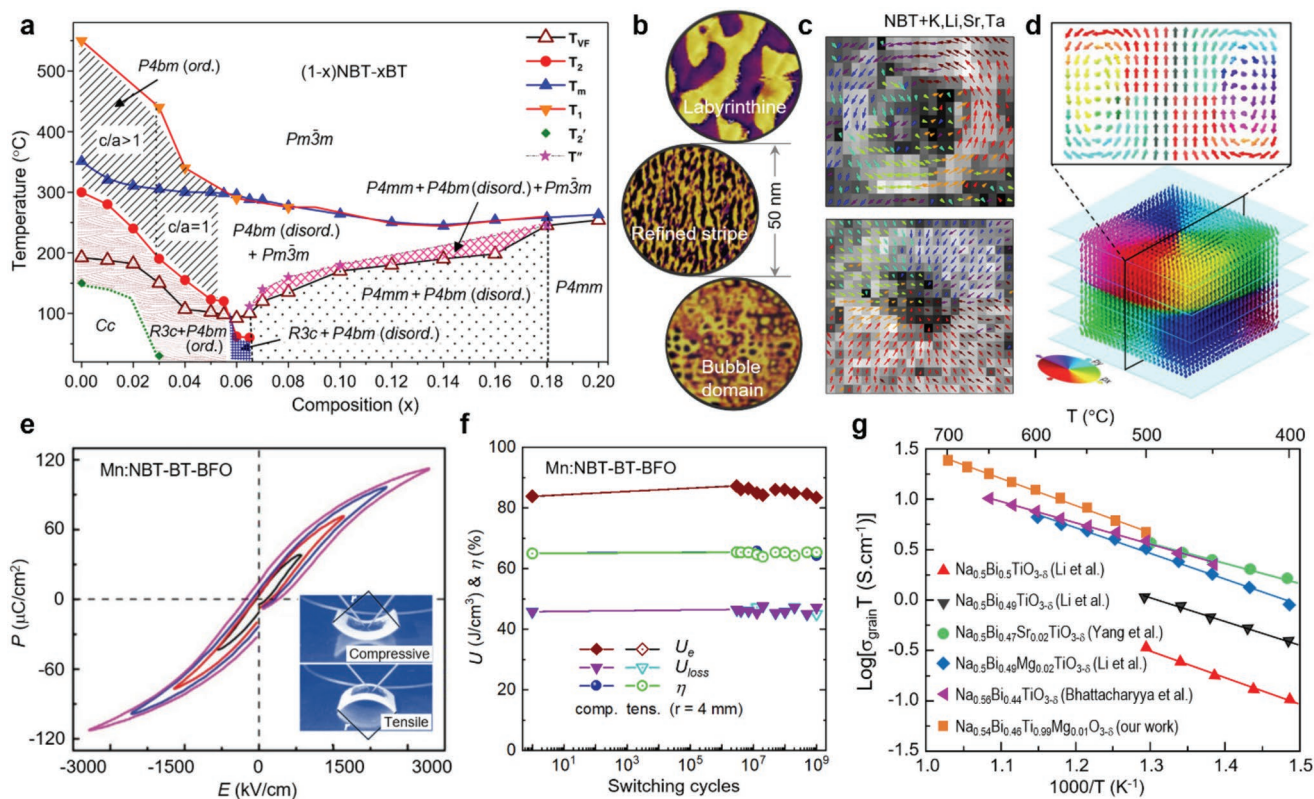


Figure 5. Phase diagram, topological structures and energy storage in $\text{Na}_{0.5}\text{Bi}_{0.5}\text{TiO}_3$ (NBT)-based ionic conductors. a) Phase diagram of unpoled $(1-x)\text{NBT}-x\text{BT}$ with annotation of Vogel–Fulcher freezing temperature (T_{VF}), rhombohedral-to-tetragonal transition (T_2), maximum dielectric permittivity (T_m), tetragonal-to-cubic transitions (T_1 , T_1') and onset temperature of in-phase octahedral tilt (T_2'). Reproduced with permission.^[137] Copyright 2021, American Physical Society. b–d) PFM phase images of chemically (K, Li, Sr, Ta doping) driven domain evolution, flux-closure circinate and hedgehog-like skyrmions and 3D representation of a polar skyrmions in bulk NBT-based ferroelectrics, respectively. Reproduced according to the terms of the CC-BY license.^[141] Copyright 2021, The authors, published by Springer Nature. e, f) P – E loops of Au/Mn:NBT-BT-BFO/Pt capacitors on mica substrates and the recoverable energy storage (U_e), efficiency (η), and energy loss (U_{loss}) under compressive and tensile bending states (r , bent radius), respectively. Reproduced with permission.^[143] Copyright 2019, Wiley-VCH. g) Comparison of ionic conductivity of $\text{Na}_{0.5}\text{Bi}_{0.5}\text{TiO}_{2.965}$ with different kinds of chemical doping in the range of 400–700 °C. Reproduced with permission.^[146] Copyright 2018, Elsevier.

lead-free system, which also exhibits decent photovoltaic effect and photocatalytic activity in water splitting.^[131,132] As for its ground-state structure, the decades-long issue^[133] reaches a general consensus until affirmation of a monoclinic (Cc) phase,^[134,135] which arises from Na/Bi positional disorder. By suppressing this disorder via poling, the average Cc phase irreversibly transforms into the R3c phase.^[136] Apart from the Cc phase, unpoled NBT also experiences several other characteristic phases, for example, coexisting rhombohedral ($R3c$, $a^-a^-a^-$) and ordered tetragonal ($P4bm$, $a^0a^0c^+$) phases at $T_2' < T < T_2$, ordered $P4bm$ phase at $T_2 < T < T_1$ (Figure 5a). Interestingly, associated with phase coexistence, NBT traverses two characteristic relaxor temperatures, a Vogel–Fulcher freezing temperature at $T_{VF} \approx 200$ °C and a maximum dielectric permittivity at $T_m \approx 350$ °C.

Through solid solution with other systems, for example, BaTiO_3 (BT), the transition lines further extend in the phase diagram of $(1-x)\text{NBT}-x\text{BT}$, in which a morphotropic phase boundary (MPB) is identified at $x \approx 0.06$ compositional point.^[137–139] By examining atomic pair distribution functions and Raman scattering data at ambient conditions, Data et al. pointed out that the easy switchability of electric dipoles driven by polarization-strain decoupling accounts for the enhanced piezoelectricity.^[75,140] Apart from the

classic polarization rotation mechanism,^[11,51] which flattens the energy profile at the MPB, this provides another insight to understand the origin of ultrahigh piezoelectricity in perovskite oxides. Interestingly, by chemically tuning the structural phases, NBT-based ceramics show controllable domain morphologies, ranging from labyrinthine, refined stripe to bubble domains (Figure 5b–d). Using atomic-scale STEM, Yin et al. observed intriguing polar skyrmions structures with either flux-closure circinate or hedgehog-like geometries in K-Li-Sr-Ta doped NBT bulks.^[75,141] Similar to topological configurations reported in $(\text{PbTiO}_3)_m/(\text{SrTiO}_3)_n$ superlattices,^[25] the interplay of bulk, elastic and electrostatic energies might be responsible for their formation.

It has been known that the pure NBT ceramics have a square-shape P – E hysteresis loop^[131] with $P_{max} \approx 38 \mu\text{C cm}^{-2}$, which can be doubled when grown into thin films.^[142] By means of chemical modification, for example, dilute Mn doping, Yang et al., reported that the P_{max} and E_B can be increased to $113 \mu\text{C cm}^{-2}$ and 2.3 MV cm^{-1} in Mn:NBT-BT-BiFeO₃ (Mn:NBT-BT-BFO) thin films.^[143] This gives rise to a very high recoverable energy density ($U_e = 81.9 \text{ J cm}^{-3}$) with η at a value of 64.4%. Although being smaller than its record-high values ($U_e = 154 \text{ J cm}^{-3}$, $\eta \approx 97\%$),^[125] the modified NBT-BT system

exhibits superior frequency stability, broad operating window and anti-fatigue property ($\approx 1 \times 10^9$ cycles)^[143] even under bending states (Figure 5e,f). Some figures of merit are valid in NBT-based bulk capacitors as well.^[144,145] Transport property study indicates that the excellent electrical performances correlate intimately with the conductivity of NBT. On one hand, being sensitive to Bi–O vacancies, Bhattacharyya et al. showed that vacancy-doped NBT delivers an ultrahigh ionic conductivity $\approx 14.3 \text{ S cm}^{-1}$ at 600 °C in grains (Figure 5g), which is three times higher than that of 8 mol% Y_2O_3 stabilized ZrO_2 (8YSZ) and is similar to that of $1\text{CeO}_2\cdot 9\text{Sc}_2\text{O}_3\cdot 90\text{ZrO}_2$ ($1\text{Ce}_9\text{ScSZ}$).^[146] On the other hand, the polar topological structures offer a pathway of enhancing its electronic conductivity, as evidenced in ferroelectrics like BiFeO_3 .^[147,148] Therefore, referring to the superior anti-fatigue performance, one can see that the synergistic ionic and electronic conductivity yields close-to-ideal interfacial polarization screening.^[149–151] Similar to $\text{Au/SrTiO}_3/\text{LSMO}$ capacitors, this further implies that the improved energy storage performances are assisted by electric-field driven electrochemical activities.

4. Solar Energy Harvesting

4.1. Energy Harvesting Mechanism

Solar energy is the most abundant energy resource among various ones and its power that continuously strikes the Earth is more than 10 000 times of the world's total energy use. A solar cell directly converts the energy of visible light into electricity through a photovoltaic effect, where charge carriers are excited to higher energy states of the materials. To realize this, three key physical steps should take place: 1) Generating electron–hole pairs or excitons through absorption of light; 2) separation of charge carriers of opposite types; 3) extraction of separated carriers to an external circuit. Ideally, a key functional material should have a bandgap of $E_g = 1\text{--}2 \text{ eV}$ to maximize the photon absorption. For this reason, crystalline and amorphous Si, GaAs, and metal halide perovskites^[152,153] have been investigated for device industrialization. For a solar cell, power conversion efficiency (PCE) is a core parameter to evaluate its performance, which is affected by factors like^[154] reflectance, quantum efficiency, separation, and collection efficiency of charge carriers. Given the natural attributes in separating electrons and holes, ferroelectrics are constantly investigated to improve the PCE and open-circuit voltage (V_{OC}) in the past decade.^[155–157] Nowadays, hybrid organic–inorganic perovskites (HOIPs) have become the research focus due to their ideal optical property, ease of fabrication and low cost.

4.2. Hybrid Organic–Inorganic Perovskites for Solar Cells

Ever since 2009, lead halide perovskites have become a forefront of photovoltaics and optoelectronics research due to their superb optoelectronic properties.^[158,159] Accordingly, interaction of lattice instabilities pertinent to the emergence of ferroelectricity has been hotly debated owing to their structural similarity with other FE perovskites.^[74,160] So far, it is generally accepted that the exceptional PCE and high V_{OC} are attributed to the following

factors: 1) High absorption coefficient ($\alpha > 10^5 \text{ cm}^{-1}$), 2) ultra-long diffusion length and lifetime of carriers, 3) moderate carrier mobility, 4) high defect tolerance and slow carrier recombination.^[154] By means of interface engineering, the performance of HOIP solar cells has achieved a PCE of 25.6% and an operational stability up to 1400 h.^[161,162] In spite of this, debates about origin of the exceptional photovoltaic effect and nature of the charge carriers remain, which call for an in-depth mechanistic understanding about the carrier-lattice interaction,^[163,164] polaron formation,^[165,166] role of lattice polarization in photo-excited electron–hole pairs and their reduced recombination, etc.^[160,167–169]

Methylammonium lead halide MAPbI_3 ($\text{MA} = \text{CH}_3\text{NH}_3^+$, bandgap $E_g \approx 1.6 \text{ eV}$) is one of the representatives in the family of HOIPs. With lowering of temperature,^[170,171] X-ray diffraction study reveals that it undergoes a cubic-to-tetragonal ($\text{Pm}3\text{m}$ to 14cm) transition at 327 K and a tetragonal-to-orthorhombic (14cm to $\text{Pna}2_1$) transition at 165 K (Figure 6a). With lattices elongated by 0.5% along c axis, the non-centrosymmetric tetragonal phase is characteristic of slightly twisted PbI_6 octahedrons.^[172] Specifically, the Rayleigh response persisting up to $\approx 348 \text{ K}$ implies that the MAPbI_3 is a relaxor FE.^[173] Associated with orienting polarization into large domains by large poling field ($>16 \text{ V cm}^{-1}$), results of scanning microwave impedance microscopy (sMIM) measured at 200 kHz and contact Kelvin probe force microscopy (cKPFM)^[173] further verify its FE polarization and switchable nature (Figure 6b). This is supported by observation of frequency dependent polarization behavior in PFM and $P\text{--}E$ loop measurements.^[174] Single-crystal X-ray diffraction reveals that polar distortion of the PbI_6 octahedra (Figure 6c), with off-center Pb shift, is responsible for presence of the intrinsic ferroelectricity.^[100,175,176]

The octahedral distortion driven FE origin is consistent with the robust ferroelectricity ($P_S = 16.13 \text{ } \mu\text{C cm}^{-2}$) identified in $\text{N}(\text{CH}_3)_4\text{SnI}_3$, in which the $\text{N}(\text{CH}_3)_4^+$ cation is nonpolar,^[177] and absence of long-lived (A)FE domains in HOIPs with polar but dynamically disordered A-site cations^[178,179] (2.29 Debye for the MA^+ cation^[167]). One should note that the out-of-phase octahedral rotations couple with the orientation of A-site cations, leading to instantaneous symmetry-broken nanostructures (1–3 nm) at room temperature and above.^[180] By strengthening the cooperative coupling, the ferroelectricity is further enhanced in 2D Ruddlesden–Popper-type HOIPs,^[181,182] for example, BA_2PbCl_4 (space group $\text{Pb}2_1\text{m}$, $E_g = 3.32 \text{ eV}$), which has vdW interlayer bonding and its polarization is $\approx 8 \text{ } \mu\text{C cm}^{-2}$ along b axis (Figure 6d). Similar to FE BaTiO_3 and LiTaO_3 ,^[64] the 2D FE HOIPs also exhibit coexisting order-disorder and displacive features owing to ordering of organic dipoles and Pb off-center displacements. Although the poor charge transport and narrow absorption band^[183] constrain the 2D HOIPs ($\text{PCE}_{\text{max}} = 19.3\%$)^[184] from being ideal solar cells, their superior stability in air and light and strengthened ferroelectricity present more insights to comprehend performance of the 3D ones and design of more stable solar cells via 2D/3D material integration.^[185]

Coupled with structural asymmetry, the Rashba splitting further supports the role of FE polarization in sunlight harvesting. Under excitation of polarized light, Liu et al. observed spin-dependent photocurrent in 2D-PEPI single crystal using terahertz transient emission spectroscopy.^[186,187] The circular photogalvanic effect not only confirms the interband excitation,

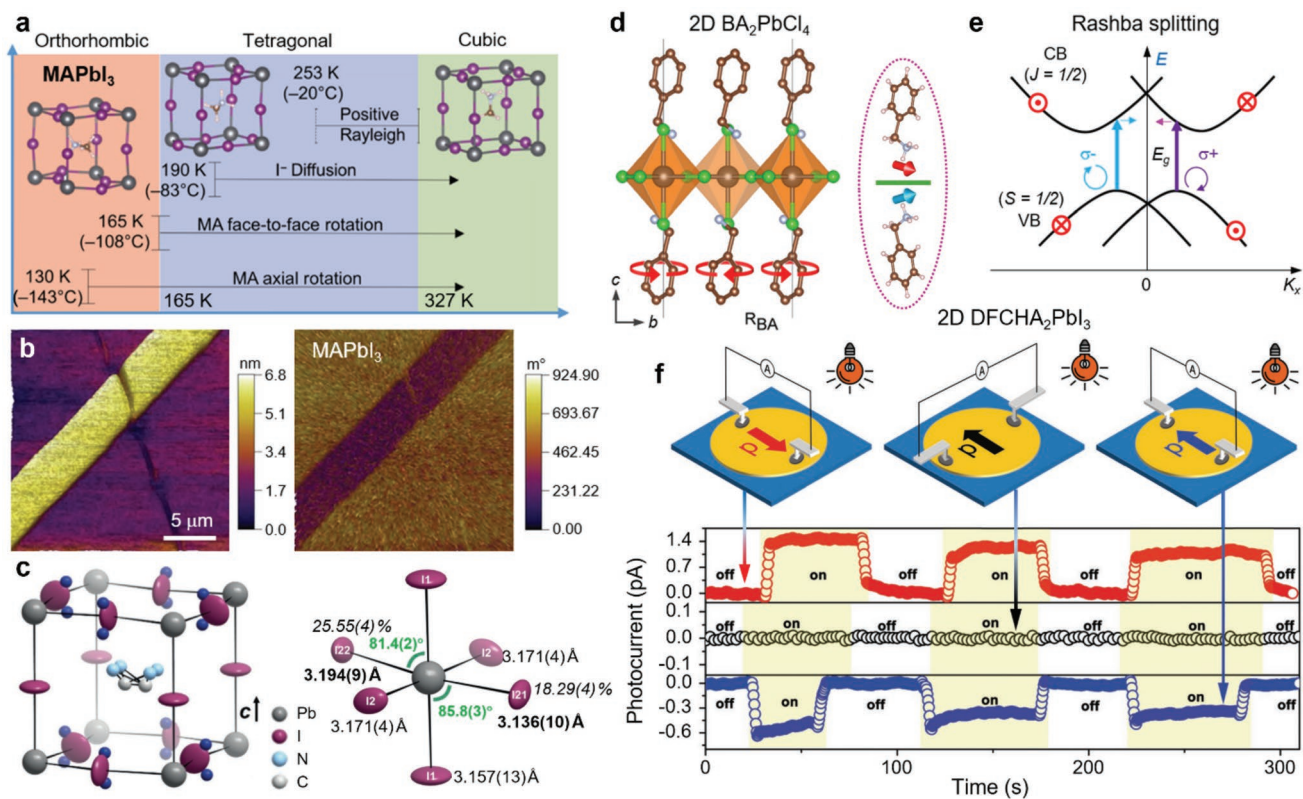


Figure 6. Ferroelectric polarization in HOIPs and device application. a) Crystal structures, temperature dependent phase transitions and Rayleigh response in MAPbI₃. b) sMIM (dC/dV) amplitude (left) and phase (right) images of MAPbI₃ showing increased and decreased signals within the positive domain. Reproduced with permission.^[173] Copyright 2019, AAAS. c) Illustration of the highest residual electron density peaks in the 2 I-site model (dark blue dots) and the PbI₆ octahedron of MAPbI₃.^[175] d) Out-of-phase rotation of the BA = C₆H₅CH₂NH₃⁺ cation and PbCl₆ octahedra as well as side view of the parallel aligned BA cations in 2D BA₂PbI₄. Reproduced with permission.^[181] Copyright 2021, American Chemical Society. e) Schematic Rashba splitting induced by spin-orbit coupling and related optical transitions with circularly polarized light. Reproduced according to the terms of the CC-BY license.^[186] Copyright 2020, The authors, published by Springer Nature. f) Ferroelectric photovoltaic measurement with different electrode and polarization configurations for the 2D (4,4-difluorocyclohexylammonium)₂PbI₄ (DFCHA₂PbI₄). Reproduced with permission.^[193] Copyright 2019, Wiley-VCH.

but also inversion symmetry breaking along out-of-plane direction of the 2D HOIP (Figure 6e). This implies that the carrier lifetime is enhanced by Rashba spin-orbit coupling in the 3D HOIPs.^[188–190] To a large degree, these structural and electrical features resemble that of relaxor FE SrTiO₃.^[112,119,124,191] To examine the role of polarization in enhancing the PCE, Xu et al. presented a typical example through introducing homochiral FE molecular into (FA_{0.95}MA_{0.05})Pb(Br_{0.1}I_{0.9})₃ (FA = [CH(NH₂)₂]⁺). Associated with enlarging the built-in field, effective separation and transportation of charge carriers, they found that the PCE can be increased from 18.28% to 21.78%.^[192] Although the 2D HOIPs are non-ideal candidates for solar energy harvesting,^[193–195] their decent optoelectronic responses make them usable in other electronic devices. Taking a fluorinated layered hybrid perovskite (4,4-difluorocyclohexylammonium)₂PbI₄ (space group Cmc2₁, E_g = 2.38 eV) as an example, Sha et al. showed that depending on the polarization-electrode configuration, the collected photocurrent exhibits polarization-dependent anisotropy (Figure 6f). This indicates that the 2D FE HOIPs can act as an anisotropic photovoltaic absorber and be used for optoelectronic sensors. Triggered by interfacial in-plane polarization, similar effect is also observed in heterogeneous WSe₂/black phosphorous bilayer.^[196]

4.3. Ferrielectric Ionic Conductor CuInP₂S₆

The study of 2D FE materials starts from exploring the thickness limit of ordinary ferroelectrics, for example, BaTiO₃ and PbTiO₃.^[197–199] Owing to the intrinsic size, surface and boundary effects, properties of 2D ferroelectrics can differ significantly from that of bulks.^[56,149,200] Stimulated by discovery of monolayer graphene, investigation of vdW-type 2D ferroelectrics^[201] such as SnTe, d1T-MoS₂, WO₂Cl₂, ReWCl₆, and BA₂PbCl₄ has become a hot research topic^[38] due to their diverse properties and potential device applications.^[193,202,203] This includes piezoelectric and photovoltaic effects, field-effect transistors, photocatalysis, etc. One should bear in mind that owing to the presence of vdW interfaces, “quantized” electric dipoles emerge within the isolated 2D FE layers. Thus, synergistic contributions of local charge redistribution, ionic displacement and even vacancy location play important roles in generating ferroelectricity.^[69,70,204,205]

Ferrielectric CuInP₂S₆, with T_C = 315 K and E_g = 1.503 eV,^[206] is a representative 2D vdW material for exploration of unusual ferroelectricity and multi-functional device applications.^[207,208] In structure, Cu and In atoms undergo opposite displacements within each layer along z direction and paired P–P atoms fill in

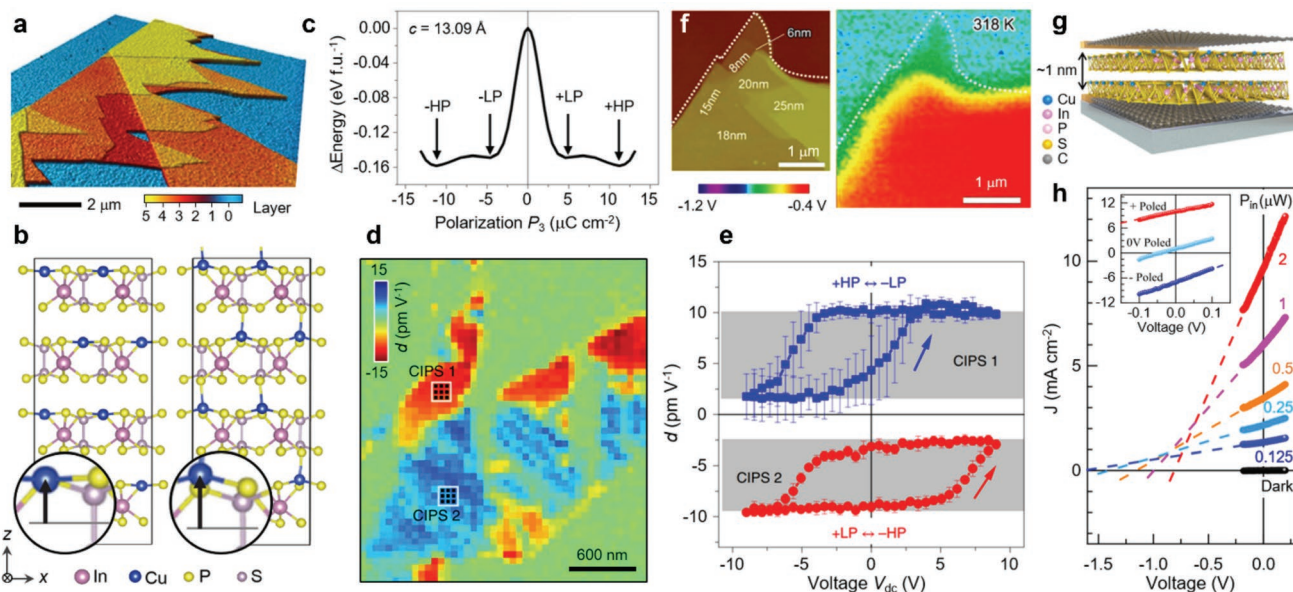


Figure 7. Crystal structure, energy landscape, and device application of CuInP_2S_6 (CIPS). a) AFM image of the CIPS flakes with different thicknesses. Reproduced according to the terms of the CC-BY license.^[209] Copyright 2016, The authors, published by Springer Nature. b) DFT calculated structure of CIPS corresponding to the first and second local energy minimum. c) Energy versus polarization relation as a function of Cu displacement per formula unit (f.u.) at $c = 13.09 \text{ \AA}$. d,e) Piezoelectric constant map and hysteresis loop as function of d.c. bias voltage averaged over a 3×3 -point grid within the two domains (CIPS 1 and CIPS 2) measured by PFM. Reproduced with permission.^[210] Copyright 2020, Springer Nature. f) AFM topography of CIPS flakes ranging from 6 to 25 nm on doped Si substrate and corresponding potential map change by heating the sample from 298 to 318 K. Reproduced with permission.^[222] Copyright 2019, Elsevier. g,h) Schematic 2D device structure and the characteristic output I - V curves under different light illumination power (P_{in}). Reproduced according to the terms of the CC-BY license.^[216] Copyright 2021, The authors, published by Springer Nature.

the sulfur cages (Figure 7a,b). Using PFM and second-harmonic generation, Liu et al. demonstrated a switchable polarization in $\approx 4 \text{ nm}$ thick CuInP_2S_6 with an on/off ratio of ≈ 100 memory behavior.^[209] By combining theoretical calculations and bias-dependent PFM experiments,^[210] Brehm et al. found that distinct from conventional proper and improper ferroelectrics, the vdW gaps enable a uniaxial quadruple potential well, which corresponds to two pairs of stable polarization values with $P_3 = \pm 4.93$ and $\pm 11.26 \mu\text{C cm}^{-2}$ (Figure 7c). As illustrated in FE polymer poly(vinylidene fluoride),^[211] the unique potential energy landscape for Cu displacements, strongly sensitive to changes of lattice constant, is responsible for its negative piezoelectric coefficient.^[212] Specifically, switching spectroscopy experiments clearly demonstrate that the two high-polarization (HP) states can individually switch to the low-polarization (LP) states, that is, from +HP to -LP and from -HP to +LP as presented in Figure 7d,e.

On the transport aspect, the ferroelectric CuInP_2S_6 also exhibits superior ionic conductivity^[213] due to the anisotropic hopping of Cu ions. Based on scanning probe microscopy (SPM) measurements, Zhang et al. revealed that the Cu ions undergo a two-step transition process, from an in-plane intra-layer hopping to an out-of-plane interlayer hopping across the vdW gaps.^[214,215] As a result, it appears that the polarization aligns against the applied electric field as Cu migrates along c axis. Using Kelvin probe force microscopy (KPFM), Niu et al. showed that ultrathin CuInP_2S_6 nanoflakes (even down to bilayer) can efficiently convert surface pyroelectric charges into electrical current as temperature changes (Figure 7f). When sandwiched by graphene electrodes (Figure 7g), Li et al. found that the photovoltaic effect of 2D CuInP_2S_6 (thickness $< 80 \text{ nm}$)

is two orders of magnitude higher than that of its bulk, FE BiFeO_3 and BaTiO_3 .^[216,217] Furthermore, the photocurrent direction, up to 9.6 mA cm^{-2} at a light illumination power of $2 \mu\text{W}$, is switchable by reversing the polarization direction (Figure 7h). These results exemplify that CuInP_2S_6 -based vdW heterostructures show great potential to convert thermal and solar energies into electricity. These facts imply that analogous to the FE $\text{Na}_{0.5}\text{Bi}_{0.5}\text{TiO}_3$, the coupling of polarization with ionic conductivity plays an important role in boosting the energy harvesting and conversion. Specifically, given the inseparable FE and electrochemical states on its surfaces, which are termed as a ferroionic state,^[218–220] the diverse coupling effects show prospects not only in suppressing recombination of photo-generated electron-hole pairs, but also in spontaneous solar-to-fuel conversion via a photocatalytic CO_2 reduction reaction (CO_2RR).^[221]

5. Electrochemical Energy Conversion

5.1. Ferroelectric-Based Catalysis

Given the challenge of supplying constant energy from fluctuating sources,^[223,224] the use of renewable energy to power the conversion of simple molecules (e.g., H_2O and CO_2) into valuable fuels and chemicals (e.g., H_2 , O_2 , ethylene, ethanol) becomes a promising strategy toward a sustainable society.^[225,226] However, many technologies are not yet industrially feasible due to the lack of robust catalysts with good performance and stability. Electrocatalysis is an energy conversion process between electrical and chemical energies, which occurs in an electrolyzer

consisting of a cathode, an anode and an acidic or alkaline electrolyte solution. Driven by an external power supply, chemical reactions take place at catalyst/reactant interfaces, where the catalysts are connected with electrodes, electron transfer and exchange participate in the energy conversion process.^[227] Due to the strong coupling of polarization to external fields and surface chemistry, FE surfaces offer exciting opportunities for the study of electrochemistry and catalytic processes such as pyrocatalysis, piezocatalysis or flexocatalysis and ferrocatalysis.^[228,229]

At the catalyst/reactant reaction interface, a strong ion versus solvent molecule interaction gives rise to a region called electrical double layer (EDL),^[230] which is comprised of an array of charged species and/or oriented dipoles near the interface.^[231] Usually, the dipolar interfacial structure can be divided into five distinct regions: 1) the electrode surface, 2) the inner Helmholtz plane (IHP), 3) the outer Helmholtz plane (OHP), 4) the diffuse layer, and 5) the bulk solution. The total thickness is in the range of 0.1–10 nm. As is known, heterogeneous catalysis on surfaces is limited by the Sabatier principle that entangles the catalytic efficiency to the optimal strength of the adsorbate-surface interaction. That is to say, the interaction has to be strong enough to drive the reaction but weak enough to permit desorption of the products.^[232] Thus, the catalytic efficiency is capped for each surface and reaction, and the search for a catalyst with the optimal active site for a given chemical reaction has been the central topic of research, which lasts for almost a century. Propelled by the limited reserves of noble metal catalysts, for example, Pt and Ir, investigation of their alternatives like carbides, sulfides, nitrides, and phosphides of transition metals offers a plethora of opportunities to explore the impact of novel electronic states on the electrochemical process.^[233]

5.2. Ferroelectric Metal WTe₂

In the family of metal chalcogenides, sulfides and selenides (e.g., MoS₂ and WSe₂) exhibit superior activity and efficiency in hydrogen evolution reaction (HER).^[233] Despite with inferior HER performance, metal tellurides such as 1T'-WTe₂ and 1T'-MoTe₂ broaden our vision to comprehend the intricate electrochemical process^[234,235] due to their exotic nonlinear anomalous Hall effect^[236] and unconventional charge-to-spin conversion.^[237] In structure, both 1T'-WTe₂ and 1T'-MoTe₂ (space group Pmn2₁)^[238–240] have vdW-type interlayer bonding and belong to type-II Weyl semimetals. In momentum space, the Weyl fermions emerge at the boundary between tilted electron and hole pockets near the Fermi energy (E_F) (Figure 8a,b).^[241] Along c axis, breaking of structural inversion symmetry simultaneously gives rise to an out-of-plane polarization. This tells that both of them are FE metals, which are a concept proposed by Anderson in 1965 and defined by coexisting ferroelectricity with metallicity.^[33–35] Albeit different in origin, the exotic electronic state is reminiscent of bent band structure caused by charged domain walls in ordinary ferroelectrics,^[242–244] where the band bending across the E_F leads to spatially separated 2D electron and hole gases (Figure 8c).

As elaborated before, ferroelectricity stems from long-range electrostatic forces, which can be annihilated by free electrons.^[245] Thus, FE metals are very rare compared with

their counterpart, FE insulators. To remedy the property disparity, one primary consideration resides in removal of inversion symmetry through displacements of atoms, whose electronic degrees of freedom are decoupled from the states at the Fermi level. Guided by this strategy, Puggioni and Rondinelli^[246] generalized three routes to lift inversion symmetry in metallic compounds: 1) Compositional order; 2) packing of acentric polyhedra; 3) geometric-induced displacements. For the 2D metal tellurides, its metallic ferroelectricity should arise from the latter two routes. To be precise, first-principles calculations show that its ferroelectricity stems from uncompensated interlayer charge transfer,^[71,247] where its in-plane direction is metallic but the electrons are confined vertically.

By sandwiching electrically contacted thin WTe₂ flakes using dielectric BN sheets (Figure 8d,e), Fei et al. explicitly demonstrated the FE switching via bistable conductance in bilayer and trilayer WTe₂.^[248] Microscopically, the polarization reversal can be attributed to re-distribution of electrons and holes and even interlayer sliding.^[69,249] The switchable polarization states are further confirmed by PFM experiments carried out on the 1T'-WTe₂ thin films^[250] (Figure 8f,g). Distinct from cycle-dependent activity decay in ordinary catalysts,^[251] the HER performance of 1T'-MoTe₂ is dramatically improved as the electrode is held at a cathodic bias,^[252] where its over-potential decreases from 320 to 178 mV at a current density of 10 mA cm⁻² (Figure 8h). This reveals that associated with adsorption of H onto surface of the Te sites, the HER activity of 1T'-MoTe₂^[252] is greatly boosted by partial filling of d -bands near the E_F and charge-to-spin conversion.^[253] Obviously, the FE metals with electrically-tunable electronic states serve as a novel template for probing efficient electrocatalysis and electrochemical energy conversion.^[202,254]

5.3. Topological Ferroelectric Metal Ni₂P

It is known that the performance of catalysts highly depends on their morphology, for example, size, shape, crystal facet, and composition. At the same time, the types and attributes of the supporting materials also play important roles in influencing their activity and selectivity.^[255] For an elemental catalyst, configuration of the reaction interface seems to be simple. Taking Au for HER as an example, the EDL geometry exhibits layer-dependent orientation discrepancy of dipolar H₂O molecules on the solution side (Figure 9a,b), which collectively vary from one-H-down to two-H-down configurations with increasing of the electric potential.^[256,257] While for a compound-type catalyst, the dynamic charge transfer process is further complicated by physical property of the catalyst itself, intercalation versus de-intercalation of certain atomic species near the catalyst surface^[258] and interfacial contact with the support.^[259]

Transition-metal phosphides such as Ni₅P₄ and Fe_{0.5}Co_{0.5}P are promising catalysts owing to their high activity and multifunctionality in catalyzing chemical reactions.^[260,261] Taking Ni₂P as an example, it is highly efficient for HER,^[262] oxygen evolution reaction (OER),^[263] CO₂RR,^[264] and hydrodesulfurization.^[265] The nonpolar Ni₂P (space group P62m) has a non-centrosymmetric structure due to the $\bar{6}$ rotational symmetry along c axis (Figure 9c). In combination with valence state measurement using electron energy loss spectroscopy (EELS), Wei et al. found

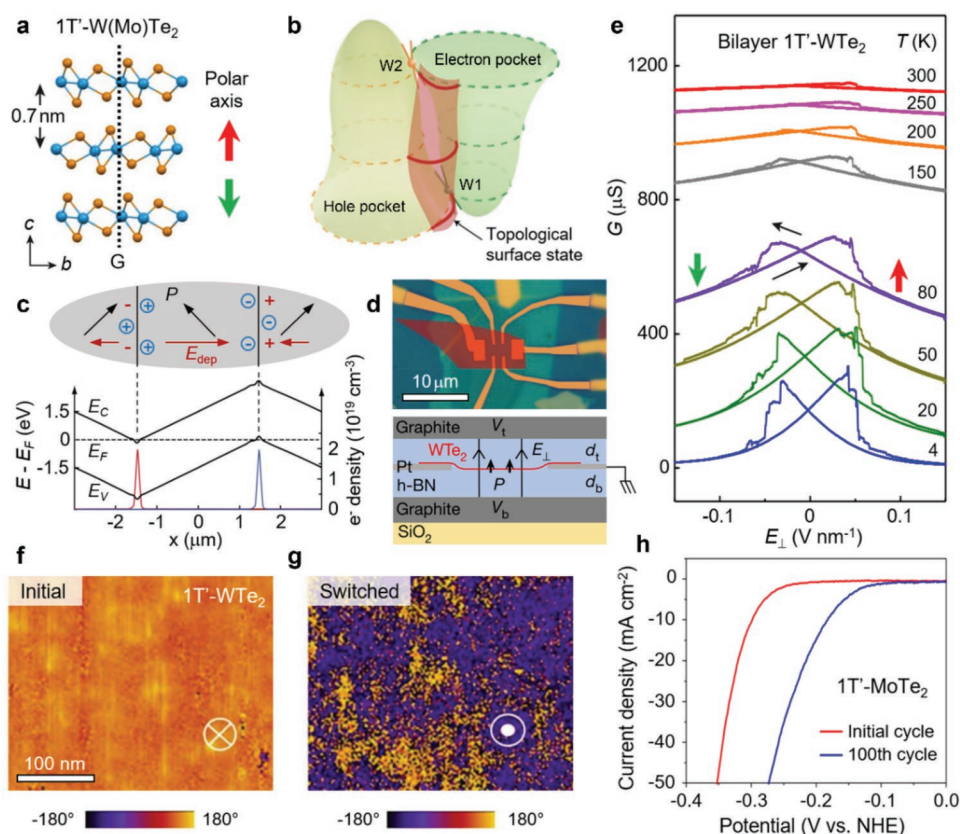


Figure 8. Ferroelectric switching in semimetal 1T'-WTe₂ and electron doping enhanced HER in 1T'-MoTe₂. a) Structure of 1T'-WTe₂ with annotation of the glide plane (G) and polarization (red, green arrows) along *c* axis (W—blue, Te—orange). b) Dispersions of Type-II Weyl fermion with electron and hole pockets touching at two different energies near the Fermi level (E_F). Reproduced with permission.^[241] Copyright 2016, Springer Nature. c) Charged planar domain walls (\oplus/\ominus : bound charges, +, -: free charges) and depolarization field (E_{dep}) induced band structure bending in ordinary ferroelectrics.^[243] d) Optical image (up) and schematic cross section of the device geometry used to apply a vertical electric field E_{\perp} normal to the WTe₂ flake. e) Temperature dependent conductance G_{gr} of bilayer WTe₂ measured when a bias V_b is applied to the bottom gate and sweeping the E_{\perp} . Reproduced with permission.^[248] Copyright 2018, Spring Nature. f,g) PFM phase images of WTe₂ before and after application of a bias pulse of -2.5 V, respectively. Reproduced according to the terms of the CC-BY license.^[250] Copyright 2019, The authors, published by AAAS. h) Current densities achieved before and after 100-cycle HER tests in 1 M H₂SO₄ for nanocrystalline 1T'-MoTe₂. Reproduced according to the terms of the CC-BY license.^[252] Copyright 2019, The authors, published by Springer Nature.

that the paramagnetic Ni₂P belongs to topological FE metal.^[266] With a winding number $n = 1$, the novel topological state is characterized by coupling of switchable in-plane polyhedral polarization, elemental valence states, Ni atomic sites and spin polarization, where the spin splitting is in the range of 20–100 meV (Figure 9d,e). Since a number of catalysts^[267–269] (e.g., Fe₂P and Ni₃S₂) exhibit similar structural features, this implies that their bulky physical properties can be further understood from the viewpoint of polyhedral polar topology (Figure 9f,g).

It is interesting to note that apart from the possible active sites for OER, for example, hydroxide/oxyhydroxide species and e_g -electron occupancy,^[270–272] it is indicated that the ultrafast polarization switching dynamics and spin-polarized kinetics^[112,273–275] also contribute a lot to the water oxidation. For metallic Ni₂P, only ≈ 5 pm Ni displacements can transform a center-convergent topological geometry to a center-divergent one (Figure 9d). With consideration of atomic Debye-Waller factors,^[276] $B = \frac{8\pi^2}{3} \langle u^2 \rangle$ ($\langle u^2 \rangle$ is mean squared displacement), the much larger Ni displacement in the range of 11–16 pm implies that the topological transition takes place at a frequency

of normal lattice vibration, that is., $\approx 10^{13}$ Hz, which should be weakly dependent on the applied voltage. Such a dynamic boosting mechanism is supported by a number of theoretical and experimental findings.

Based on first-principles calculations, Lan et al. predicted that for clean (001) and OH-covered surfaces (Figure 9h,i), the overpotential (η_{op}) values of improper FE InSnO₂N can drastically reduce from 0.58 V (downward *P*) and 0.77 V (upward *P*) to 0.20 and 0.23 V, respectively, as the polarization is dynamically switched during the OER reaction.^[277] These values are far below the minimum theoretical one of oxide catalysts ($\eta_{op} = 0.37$ V).^[278] On the experimental side, by implementing high-frequency mechanical vibration,^[279] the ultrafast polarization reversal successfully transforms the insulating BaTiO₃ and BiFeO₃ into excellent water splitting catalysts.^[44,280] Using ambient pressure X-ray photoelectron spectroscopy,^[281–283] Domingo et al. have demonstrated different water affinity, dynamics of water adsorption, dissociation and oxidation on surfaces of Pb(Zr_{0.2}Ti_{0.8})O₃, LiNbO₃ and BaTiO₃. Therefore, as an external agent to modulate surface electrochemical properties, the use of FE polarization opens a route to switchable catalysis and offers new opportunities to overcome the Sabatier

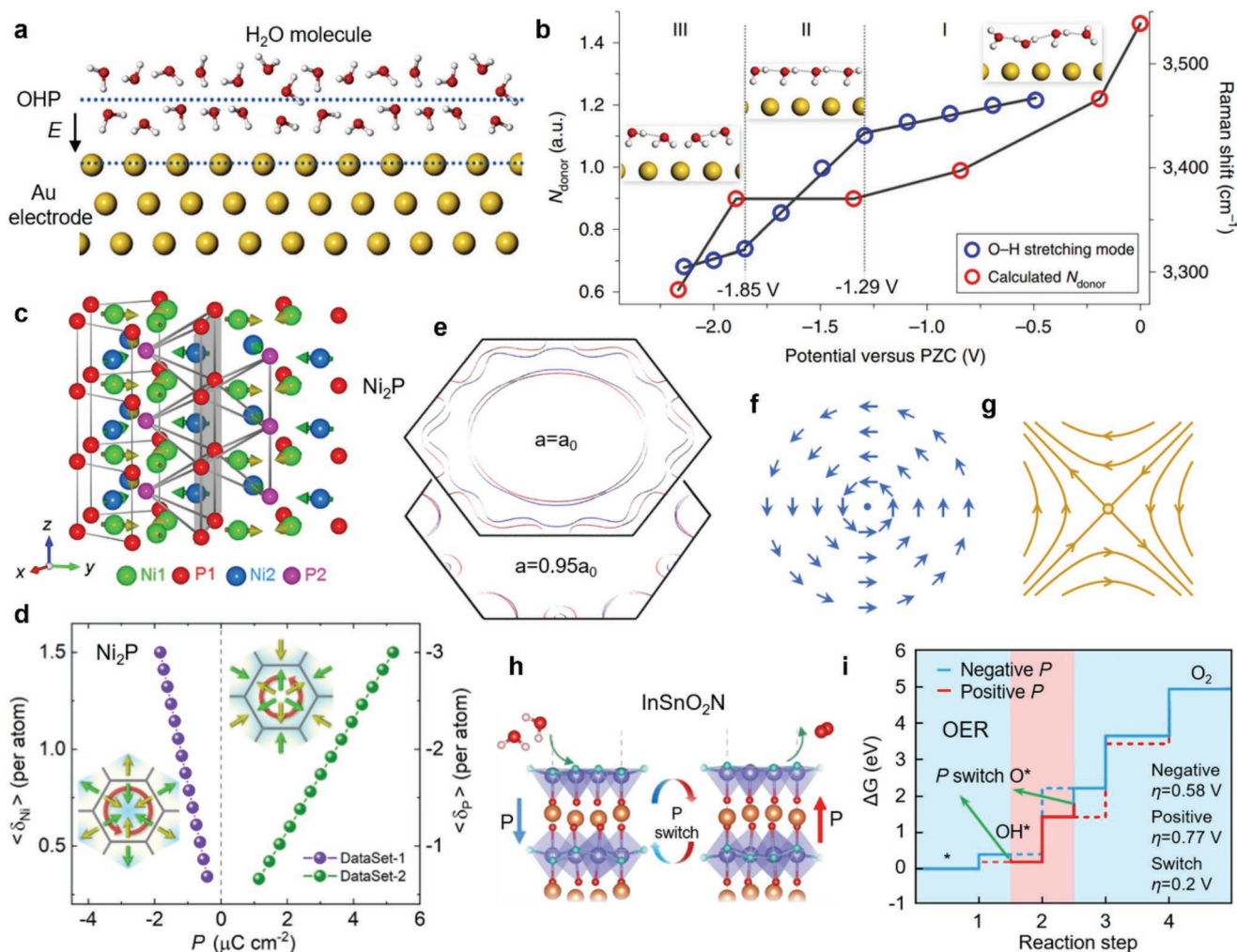


Figure 9. Impact of switchable polarization on (photo)electrochemical water splitting. a) Illustration of an EDL model and associated outer Helmholtz plane (OHP) under electric field (E). b) Potential-dependent evolution of hydrogen-bonded network of interfacial H_2O molecules from calculation (N_{donor} , number of H-bond donors) and experimental Raman frequency $\nu_{\text{O-H}}$ (blue circle). Reproduced with permission.^[256] Copyright 2019, Springer Nature. c,d) Tail-to-tail polyhedral polarity in Ni_2P and in-plane topological polarization configuration (center-convergent vs center-divergent, $n = 1$) as a function of mean $\langle \delta_{\text{Ni}} \rangle$ and $\langle \delta_{\text{P}} \rangle$ for two structural data sets, respectively. e) In-plane compressive strain ($a/a_0 = 1.0, 0.95$) induced Fermi surface change on a plane in the Brillouin zone (Blue—spin up, red—spin down along z axis). Reproduced according to the terms of the CC-BY license.^[266] Copyright 2020, The authors, published by Wiley-VCH. f,g) 2D topological point defects about polarization or spin with $n = 1$ and -1 , respectively. Reproduced with permission.^[286] Copyright 1979, American Physical Society. h,i) Polarization switching and Gibbs free energy diagram of OER steps for clean (001) surface of improper ferroelectric InSnO_2N , respectively. Reproduced with permission.^[277] Copyright 2021, American Chemical Society.

limitations with consideration of issues about surface adsorption, charge carrier separation, redox reactions, etc.^[284,285]

5.4. vdW Ferroelectric $\alpha\text{-In}_2\text{Se}_3$

Besides (photo)electrochemical water splitting,^[287] electrochemical CO_2RR provides another pathway to convert electric energy into chemical fuels, for example, methane (CH_4), ethylene (C_2H_4), methanol (CH_3OH), and ethanol ($\text{C}_2\text{H}_5\text{OH}$).^[226,288] It is known that Cu-based materials are efficient catalysts for CO_2RR . However, they suffer from issues like low activity and selectivity, insufficient Faradaic efficiency and poor durability.^[226] For this reason, many efforts have been made to develop new catalysts such as Ag-based catalysts for high-selectivity conversion of butanol and hexanol,^[288] nickel phosphides (Ni_2P , Ni_3P_4 ,

and NiP_2) for unprecedented selectivity of C_3 and C_4 oxyhydrocarbon products,^[264] single-atom-catalyst (SAC) Zn for highly efficient CH_4 conversion.^[289] Apart from these, FE materials such as $\text{SrBi}_4\text{Ti}_4\text{O}_{15}$, Bi_2MoO_6 , and CuInP_2S_6 have also been used for CO_2 photocatalytic reduction given their tunable activity and selectivity.^[221,290,291]

Among various layered vdW ferroelectrics,^[38] for example, $\text{d}1\text{T-MoS}_2$, GeSn , and CrN , a class of $\text{III}_2\text{-VI}_3$ semiconductors represented by In_2Se_3 have attracted a great deal of attention due to its exceptional optical properties.^[292,293] The In_2Se_3 is polymorphic with many structural phases (α' , α , β , β' , γ , δ , κ),^[294] in which the α , β , and β' phases are of vdW type and are differed by 2H, 3R, and 1T stacking on the $[\text{Se-In-Se-In-Se}]$ quintuple layers (QLs).^[295] Specifically, the $\alpha\text{-In}_2\text{Se}_3$ phase (space group $R3m$) with a ZB' structure has aroused intensive discussions on its intriguing FE property^[296–298] and potential

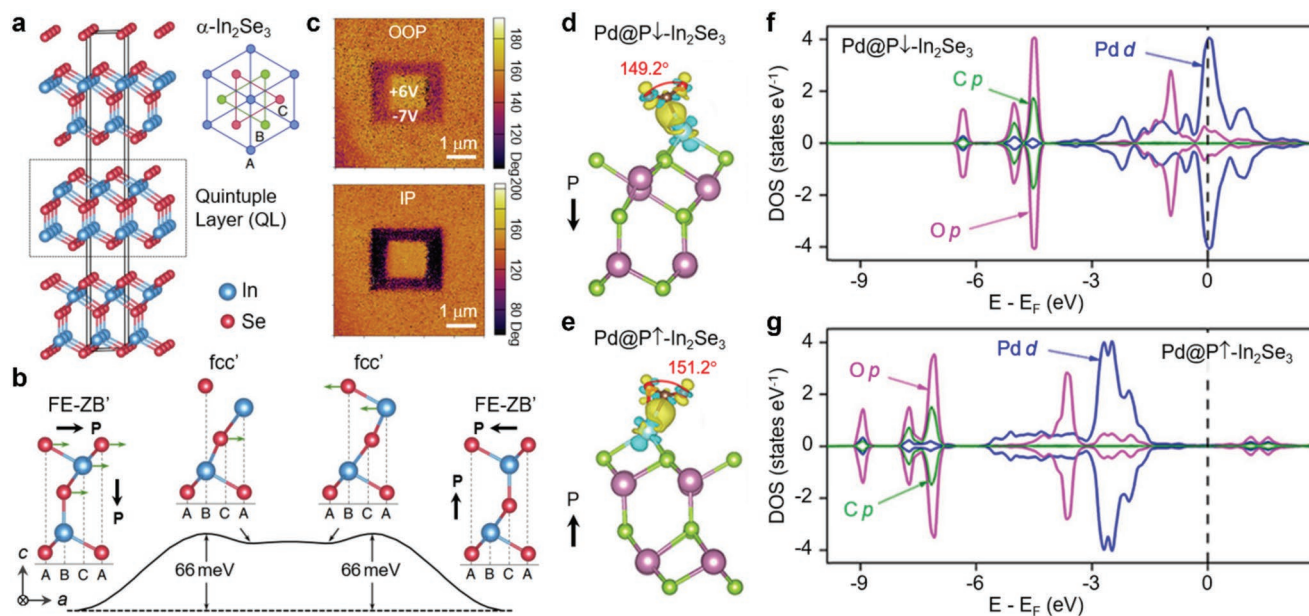


Figure 10. Ferroelectric switching and controllable CO₂ reduction on single atom anchored α -In₂Se₃. a) Crystal structure of 2D In₂Se₃ quintuple layers (QLs) linked by van der Waals gaps along vertical z direction. Each type of atom arranges only in one of the triangular (A, B, or C) lattices. b) Effective kinetic pathway of polarization reversal in one QL In₂Se₃ (ZB': stabilized zincblende (ZB) structure) through a metastable face-centered cubic (fcc') phase. Reproduced with permission.^[301] Copyright 2018, American Chemical Society. c) Out-of-plane (OOP) and in-plane (IP) PFM phase images of 6 nm thick In₂Se₃ flake acquired consecutively at -7 and +6 V voltages. Reproduced with permission.^[302] Copyright 2018, American Chemical Society. d-g) Differential charge density plots (In-purple, Se-green) and partial density of states of CO₂ adsorbed on Pd@P↓-In₂Se₃ (d,e) and Pd@P↑-In₂Se₃ (f,g), respectively. Reproduced according to the terms of the CC-BY license.^[306] Copyright 2021, The authors, published by Springer Nature.

device application.^[299,300] Distinct from the displacive and order-disorder ferroelectrics, the polarization in α -In₂Se₃ is reversed through synergistic lateral shifts of top three atomic layers in one QL, which experiences a metastable face-centered cubic (fcc') phase^[301] and the energy barrier is about 66 meV (Figure 10a-c). As corroborated by PFM experiments, the 2D α -In₂Se₃ exhibit inter-correlated in-plane and out-of-plane polarization components.^[302,303]

Because of having large surface-to-volume ratio, short carrier diffusion length and unique electronic properties, 2D materials serve as promising substrates for SACs.^[304,305] Inspired by the ideal surface geometry, Ju et al. predicted that the catalytic activity and selectivity of transition-metal atoms anchored α -In₂Se₃ (TM@In₂Se₃, TM = Ni, Pd, Rh, Nb, or Re) used for CO₂RR can be controlled by FE switching through adjusting the *d*-band center and occupation of supported metal atoms.^[306,307] By forming bidentate C-TM-O species, the strong hybridization of O *p* and TM *d* orbitals and charge transfer ensure chemical capture of the inert CO₂ on the TM@In₂Se₃ surfaces. The activation degrees on opposite FE surfaces are manifested by different \angle OCO angles of the CO₂ molecules (Figure 10d,e). Specifically, the switchable polarization effectively modulates the *d* orbital occupation of the TM atoms, which further control the reaction barrier, reaction path, and even the intermediate/final product of CO₂RR (Figure 10f,g).

6. Summary and Outlook

In conclusion, we reviewed the origin of ferroelectricity and summarized the latest research progress about novel FE materials

used for energy harvesting, storage, and conversion. From the typical perovskite oxides, one can see that the polarization-related phenomenon has conspicuously extended to HOIPs, 2D vdW-layered materials, metals, ionic conductors, etc. The physics underpinning these phenomena involves the intricate interplay of polarization with geometric coordination, defect, electron correlation and spin state under either static or dynamic conditions. Towards building a clearer structure-property relationship and maximizing performance of the materials, several guidelines for carrying out FE energy research are generalized as follows.

- 1) As exemplified by PbZrO₃-, SrTiO₃-, and NBT-BT-based systems, exploring cross-scale characterization and transient structural transitions under in-situ biasing conditions^[100] represent two significant directions for dielectric capacitor research. Although the physical processes dominate, electrochemical activities relating to ionic migration via defects and interfaces^[126] should play important roles in improving the storage performance of the dielectric capacitors.
- 2) Order-disorder transition of A-site organic cations,^[308] built-in field effect^[309] and charge-to-spin conversion in 3D HOIPs play essential roles in affecting the electron-hole separation and carrier lifetime in solar cells. In conjunction with annihilation of structural defects by material engineering,^[310] it is believed that unraveling the structural mysteries of HOIPs under working conditions using atomically-resolved cryo-TEM^[311] can help to further improve their PEC and stability.
- 3) Case studies about 1T'-WTe₂ and Ni₂P highlight that besides the critical surface structures, understanding the inherent bulky attributes of the transition-metal catalysts^[312] also play important roles in probing their energy conversion

mechanisms. Although aspects like spin-to-charge conversion can hardly be accessed during the reaction, adoption of operando scanning transmission X-ray microscopy (STXM)^[258] and cryo-STEM promise to unveil more concrete in-situ interfacial information about crystal, chemical and electronic structures.

- 4) Either homogeneous or heterogeneous, 2D vdW-layered materials offer us great opportunities to design energy-related devices by stacking layers with a variable twist angle at quasi-equilibrium configurations.^[313,314] Due to limitations from discrete physical boundary conditions, nontrivial physical properties absent in the parent compounds can emerge and novel interfacial polarization is awaiting to be explored in a number of nonpolar materials.

Taking into account that a variety of factors are becoming more and more important in producing ferroelectricity, new phenomena and new physics pertinent to chemical defect, topological state of matter, ionic migration, surface and interfacial interlayer coupling are emerging rapidly and universally. Accordingly, these new properties enable us to extend the application of ferroelectrics to the field of energy-related harvesting, storage, and conversion, including solar cells, water splitting, CO₂ reduction, super-capacitors.^[315] Li-ion and Na-ion batteries,^[316–318] solid oxide fuel cells,^[319] etc. Since the polarization switching dynamics plays a significant role in the energy-related devices, exploration of various polar and electronic structures by developing operando and in-situ microscopy and spectroscopy techniques is highly desired to boost the advancement of the booming FE materials. Meanwhile, a joint effort in material design and mechanistic understanding at the atomic and molecular levels of physics and electrochemistry will be required to promote this emerging field toward industrial application in the future.

Acknowledgements

X.-K.W. acknowledges support by the Deutsche Forschungsgemeinschaft (DFG; German Research Foundation) under Germany's Excellence Strategy-Cluster of Excellence Matter and Light for Quantum Computing (ML4Q) EXC 2004/1-390534769. N.D. acknowledges financial support from the Spanish Ministerio de Ciencia e Innovación (MICINN) under project PID2019-109931GB-I00. The ICN2 was supported by the Severo Ochoa Centres of Excellence Programme, funded by the Spanish Research Agency (AEI, Grant No. SEV-2017-0706).

Open Access funding enabled and organized by Projekt DEAL.

Conflict of Interest

The authors declare no conflict of interest.

Author Contributions

X.-K.W. conceived the idea and wrote the manuscript with input from N.D., Y.S. and N.B. commented and revised the manuscript together with R.E.D.-B. and J.M., who provided full support on the scientific research. All authors have read and agreed to the published version of the manuscript.

Keywords

capacitors, CO₂ reduction, ferroelectric energy materials, solar cells, water splitting

Received: April 8, 2022
Published online: May 11, 2022

- [1] J. Valasek, *Phys. Rev.* **1921**, 17, 475.
- [2] G. Busch, *Ferroelectrics* **1987**, 74, 267.
- [3] G. Busch, P. Scherrer, *Naturwissenschaften* **1935**, 23, 737.
- [4] C. A. Randall, R. E. Newnham, L. E. Cross, *History of the First Ferroelectric Oxide BaTiO₃*, <https://ceramics.org/> (accessed: September 2021).
- [5] W. Martienssen, H. Warlimont, *Springer Handbook of Condensed Matter and Materials Data*, Springer, Berlin Heidelberg **2005**.
- [6] Y. Shiozaki, E. Nakamura, T. Mitsui, *Ferroelectrics and Related Substances*, Landolt-Börnstein New Series, Vol. III/36, Springer-Verlag, Berlin **2006**.
- [7] J. F. Scott, *Science* **2007**, 315, 954.
- [8] W. Zhang, R. G. Xiong, *Chem. Rev.* **2012**, 112, 1163.
- [9] S. Pandya, J. Wilbur, J. Kim, R. Gao, A. Dasgupta, C. Dames, L. W. Martin, *Nat. Mater.* **2018**, 17, 432.
- [10] D. Damjanovic, *Rep. Prog. Phys.* **1998**, 61, 1267.
- [11] C. Qiu, B. Wang, N. Zhang, S. Zhang, J. Liu, D. Walker, Y. Wang, H. Tian, T. R. Shrout, Z. Xu, L. Q. Chen, F. Li, *Nature* **2020**, 577, 350.
- [12] P. Khanchaitit, K. Han, M. R. Gadinski, Q. Li, Q. Wang, *Nat. Commun.* **2013**, 4, 2845.
- [13] F. Li, D. Lin, Z. Chen, Z. Cheng, J. Wang, C. Li, Z. Xu, Q. Huang, X. Liao, L. Q. Chen, T. R. Shrout, S. Zhang, *Nat. Mater.* **2018**, 17, 349.
- [14] F. Li, M. J. Cabral, B. Xu, Z. Cheng, E. C. Dickey, J. M. LeBeau, J. Wang, J. T. Luo, Samuel, W. Hackenberger, L. Bellaiche, Z. Xu, L.-Q. Chen, T. R. Shrout, S. Zhang, *Science* **2019**, 364, 264.
- [15] G. Subramanyam, M. W. Cole, N. X. Sun, T. S. Kalkur, N. M. Sbrockey, G. S. Tompa, X. Guo, C. Chen, S. P. Alpay, G. A. Rossetti, K. Dayal, L.-Q. Chen, D. G. Schlom, *J. Appl. Phys.* **2013**, 114, 191301.
- [16] V. Garcia, M. Bibes, *Nat. Commun.* **2014**, 5, 4289.
- [17] N. Setter, D. Damjanovic, L. Eng, G. Fox, S. Gevorgian, S. Hong, A. Kingon, H. Kohlstedt, N. Y. Park, G. B. Stephenson, I. Stolitchnov, A. K. Tagantsev, D. V. Taylor, T. Yamada, S. Streiffner, *J. Appl. Phys.* **2006**, 100, 051606.
- [18] P. Murali, *Rep. Prog. Phys.* **2001**, 64, 1339.
- [19] F. DeFlaviis, N. G. Alexopoulos, O. M. Stafsudd, *IEEE Trans. Microwave Theory Tech.* **1997**, 45, 963.
- [20] N. Ledermann, P. Murali, J. Baborowski, S. Gentil, K. Mukati, M. Cantoni, A. Seifert, N. Setter, *Sens. Actuators, A* **2003**, 105, 162.
- [21] K. R. Udayakumar, S. F. Bart, A. M. Flynn, J. Chen, L. S. Tavrow, L. E. Cross, R. A. Brooks, D. J. Ehrlich, in Proc. IEEE MEMS, IEEE, Piscataway, NJ **1991**, pp. 109–113.
- [22] N. Ledermann, J. Baborowski, A. Seifert, B. Willing, S. Hiboux, P. Murali, N. Setter, M. Forster, *Integr. Ferroelectr.* **2006**, 35, 177.
- [23] S. H. Wemple, M. DiDomenico, *J. Appl. Phys.* **1969**, 40, 735.
- [24] H. Zhang, T. Wei, Q. Zhang, W. Ma, P. Fan, D. Salamon, S.-T. Zhang, B. Nan, H. Tan, Z.-G. Ye, *J. Mater. Chem. C* **2020**, 8, 16648.
- [25] S. Chen, S. Yuan, Z. Hou, Y. Tang, J. Zhang, T. Wang, K. Li, W. Zhao, X. Liu, L. Chen, L. W. Martin, Z. Chen, *Adv. Mater.* **2020**, 33, 2000857.
- [26] X.-K. Wei, A. K. Tagantsev, A. Kvasov, K. Roleder, C.-L. Jia, N. Setter, *Nat. Commun.* **2014**, 5, 3031.
- [27] P. S. Bednyakov, B. I. Sturman, T. Sluka, A. K. Tagantsev, P. V. Yudin, *Npj Comput. Mater.* **2018**, 4, 65.

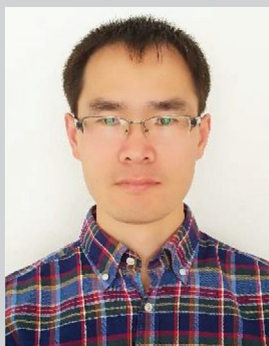
- [28] Z. Huang, Ariando, X. Renshaw Wang, A. Rusydi, J. Chen, H. Yang, T. Venkatesan, *Adv. Mater.* **2018**, *30*, 1802439.
- [29] X.-K. Wei, Y. Su, Y. Sui, Z. Zhou, Y. Yao, C. Jin, R. Yu, *Appl. Phys. Lett.* **2013**, *102*, 242910.
- [30] D. V. Christensen, Y. Frenkel, Y. Z. Chen, Y. W. Xie, Z. Y. Chen, Y. Hikita, A. Smith, L. Klein, H. Y. Hwang, N. Pryds, B. Kalisky, *Nat. Phys.* **2018**, *15*, 269.
- [31] S. W. Cheong, M. Mostovoy, *Nat. Mater.* **2007**, *6*, 13.
- [32] S. Ning, A. Kumar, K. Klyukin, E. Cho, J. H. Kim, T. Su, H. S. Kim, J. M. LeBeau, B. Yildiz, C. A. Ross, *Nat. Commun.* **2021**, *12*, 4298.
- [33] P. W. Anderson, E. I. Blount, *Phys. Rev. Lett.* **1965**, *14*, 217.
- [34] Y. G. Shi, Y. F. Guo, X. Wang, A. J. Princep, D. Khalyavin, P. Manuel, Y. Michiue, A. Sato, K. Tsuda, S. Yu, M. Arai, Y. Shirako, M. Akaogi, N. L. Wang, K. Yamaura, A. T. Boothroyd, *Nat. Mater.* **2013**, *12*, 1023.
- [35] A. Filippetti, V. Fiorentini, F. Ricci, P. Delugas, J. Iniguez, *Nat. Commun.* **2016**, *7*, 11211.
- [36] H. Zeng, J. Dai, W. Yao, D. Xiao, X. Cui, *Nat. Nanotechnol.* **2012**, *7*, 490.
- [37] Z. Zhu, A. Collaudin, B. Fauqué, W. Kang, K. Behnia, *Nat. Phys.* **2011**, *8*, 89.
- [38] M. Wu, P. Jena, *Wiley Interdiscip. Rev. Computat. Mol. Sci.* **2018**, *8*, e1365.
- [39] Z. Zheng, Q. Ma, Z. Bi, S. de la Barrera, M. H. Liu, N. Mao, Y. Zhang, N. Kiper, K. Watanabe, T. Taniguchi, J. Kong, W. A. Tisdale, R. Ashoori, N. Gedik, L. Fu, S. Y. Xu, P. Jarillo-Herrero, *Nature* **2020**, *588*, 71.
- [40] X. Wang, C. Zhu, Y. Deng, R. Duan, J. Chen, Q. Zeng, J. Zhou, Q. Fu, L. You, S. Liu, J. H. Edgar, P. Yu, Z. Liu, *Nat. Commun.* **2021**, *12*, 1109.
- [41] L. Wu, A. Wang, J. Shi, J. Yan, Z. Zhou, C. Bian, J. Ma, R. Ma, H. Liu, J. Chen, Y. Huang, W. Zhou, L. Bao, M. Ouyang, S. J. Pennycook, S. T. Pantelides, H. J. Gao, *Nat. Nanotechnol.* **2021**, *16*, 882.
- [42] J. W. Lee, H. S. Kim, N. G. Park, *Acc. Chem. Res.* **2016**, *49*, 311.
- [43] Prateek, V. K. Thakur, R. K. Gupta, *Chem. Rev.* **2016**, *116*, 4260.
- [44] H. You, Z. Wu, L. Zhang, Y. Ying, Y. Liu, L. Fei, X. Chen, Y. Jia, Y. Wang, F. Wang, S. Ju, J. Qiao, C. H. Lam, H. Huang, *Angew. Chem., Int. Ed.* **2019**, *58*, 11779.
- [45] A. Kakekhani, S. Ismail-Beigi, *ACS Catal.* **2015**, *5*, 4537.
- [46] H. Yu, F. Chen, X. Li, H. Huang, Q. Zhang, S. Su, K. Wang, E. Mao, B. Mei, G. Mul, T. Ma, Y. Zhang, *Nat. Commun.* **2021**, *12*, 4594.
- [47] B. Noheda, D. E. Cox, G. Shirane, J. A. Gonzalo, L. E. Cross, S. E. Park, *Appl. Phys. Lett.* **1999**, *74*, 2059.
- [48] X.-K. Wei, C.-L. Jia, T. Sluka, B.-X. Wang, Z.-G. Ye, N. Setter, *Nat. Commun.* **2016**, *7*, 12385.
- [49] A. K. Kalyani, D. K. Khatua, B. Loukya, R. Datta, A. N. Fitch, A. Senyshyn, R. Ranjan, *Phys. Rev. B* **2015**, *91*, 104104.
- [50] Z. Chen, S. Prosdaveev, Z. L. Luo, W. Ren, Y. Qi, C. W. Huang, L. You, C. Gao, I. A. Kornev, T. Wu, J. Wang, P. Yang, T. Sritharan, L. Bellaiche, L. Chen, *Phys. Rev. B* **2011**, *84*, 094116.
- [51] H. Fu, R. E. Cohen, *Nature* **2000**, *403*, 281.
- [52] E. Aksel, J. L. Jones, *Sensors* **2010**, *10*, 1935.
- [53] D. D. Fong, G. B. Stephenson, S. K. Streiffer, J. A. Eastman, O. Auciello, P. H. Fuoss, C. Thompson, *Science* **2004**, *304*, 1650.
- [54] P. Gao, Z. Zhang, M. Li, R. Ishikawa, B. Feng, H. J. Liu, Y. L. Huang, N. Shibata, X. Ma, S. Chen, J. Zhang, K. Liu, E. G. Wang, D. Yu, L. Liao, Y. H. Chu, Y. Ikuhara, *Nat. Commun.* **2017**, *8*, 15549.
- [55] K. Change, J. Liu, H. Lin, N. Wang, Z. Kun, A. Zhang, F. Jin, Y. Zhong, X. Hu, W. Duan, Q. Zhang, L. Fu, Q.-K. Xue, X. Chen, S.-H. Ji, *Science* **2016**, *353*, 274.
- [56] C. L. Jia, V. Nagarajan, J. Q. He, L. Houben, T. Zhao, R. Ramesh, K. Urban, R. Waser, *Nat. Mater.* **2007**, *6*, 64.
- [57] T. Qi, I. Grinberg, A. M. Rappe, *Phys. Rev. B* **2010**, *82*, 134113.
- [58] A. Bussmann-Holder, H. Beige, G. Völkel, *Phys. Rev. B* **2009**, *79*, 184111.
- [59] A. Bencan, E. Oveisi, S. Hashemizadeh, V. K. Veerapandian, T. Hoshina, T. Rojac, M. Deluca, G. Drazic, D. Damjanovic, *Nat. Commun.* **2021**, *12*, 3509.
- [60] M. Si, X. Lyu, P. D. Ye, *ACS Appl. Electron. Mater.* **2019**, *1*, 745.
- [61] N. A. Hill, *J. Phys. Chem. B* **2000**, *104*, 6694.
- [62] R. E. Cohen, *Nature* **1992**, *358*, 136.
- [63] E. A. Stern, *Phys. Rev. Lett.* **2004**, *93*, 037601.
- [64] K. A. Müller, Y. Luspin, J. L. Servoin, F. Gervais, *J. Phys. Lett.* **1982**, *43*, 537.
- [65] D. Lee, H. Lu, Y. Gu, S.-Y. Choi, S.-D. Li, S. Ryu, T. R. Paudel, K. Song, E. Mikheev, S. Lee, S. Stemmer, D. A. Tenne, S. H. Oh, E. Y. Tsymbal, X. Wu, L.-Q. Chen, A. Gruverman, C. B. Eom, *Science* **2015**, *349*, 1314.
- [66] K. Klyukin, V. Alexandrov, *Phys. Rev. B* **2017**, *95*, 035301.
- [67] R. Gao, S. E. Reyes-Lillo, R. Xu, A. Dasgupta, Y. Dong, L. R. Dedon, J. Kim, S. Saremi, Z. Chen, C. R. Serrao, H. Zhou, J. B. Neaton, L. W. Martin, *Chem. Mater.* **2017**, *29*, 6544.
- [68] L. J. McGilly, A. Kerelsky, N. R. Finney, K. Shapovalov, E.-M. Shih, A. Ghiotto, Y. Zeng, S. L. Moore, W. Wu, Y. Bai, K. Watanabe, T. Taniguchi, M. Stengel, L. Zhou, J. Hone, X. Zhu, D. N. Basov, C. Dean, C. E. Dreyer, A. N. Pasupathy, *Nat. Nanotechnol.* **2020**, *15*, 580.
- [69] M. V. Stern, Y. Waschitz, W. Cao, I. Nevo, K. Watanabe, T. Taniguchi, E. Sela, M. Urbakh, O. Hod, M. Ben Shalom, *Science* **2021**, *372*, 1462.
- [70] K. Yasuda, X. Wang, K. Watanabe, T. Taniguchi, P. Jarillo-Herrero, *Science* **2021**, *372*, 1458.
- [71] X. Liu, Y. Yang, T. Hu, G. Zhao, C. Chen, W. Ren, *Nanoscale* **2019**, *11*, 18575.
- [72] J. R. Kim, J. Jang, K. J. Go, S. Y. Park, C. J. Roh, J. Bonini, J. Kim, H. G. Lee, K. M. Rabe, J. S. Lee, S. Y. Choi, T. W. Noh, D. Lee, *Nat. Commun.* **2020**, *11*, 4944.
- [73] X. K. Wei, T. Zou, F. Wang, Q. H. Zhang, Y. Sun, L. Gu, A. Hirata, M. W. Chen, Y. Yao, C. Q. Jin, R. C. Yu, *J. Appl. Phys.* **2012**, *111*, 073904.
- [74] M. E. Lines, A. M. Glass, *Principles and Applications of Ferroelectrics and Related Materials*, Oxford University Press, Oxford **1977**.
- [75] X.-K. Wei, S. Prokhorenko, B.-X. Wang, Z. Liu, Y.-J. Xie, Y. Nahas, C.-L. Jia, R. E. Dunin-Borkowski, J. Mayer, L. Bellaiche, Z.-G. Ye, *Nat. Commun.* **2021**, *12*, 5322.
- [76] S. V. Kalinin, N. A. Spaldin, *Science* **2013**, *341*, 858.
- [77] L. Yang, X. Kong, F. Li, H. Hao, Z. Cheng, H. Liu, J.-F. Li, S. Zhang, *Prog. Mater. Sci.* **2019**, *102*, 72.
- [78] M. Acharya, E. Banyas, M. Ramesh, Y. Jiang, A. Fernandez, A. Dasgupta, H. Ling, B. Hanrahan, K. Persson, J. B. Neaton, L. W. Martin, *Adv. Mater.* **2021**, *33*, 2105967.
- [79] C. Hou, W. Huang, W. Zhao, D. Zhang, Y. Yin, X. Li, *ACS Appl. Mater. Interfaces* **2017**, *9*, 20484.
- [80] F. Z. Yao, Q. Yuan, Q. Wang, H. Wang, *Nanoscale* **2020**, *12*, 17165.
- [81] V. Veerapandian, F. Benes, T. Gindel, M. Deluca, *Materials* **2020**, *13*, 5742.
- [82] H. Pan, S. Lan, S. Xu, Q. Zhang, H. Yao, Y. Liu, F. Meng, E.-J. Guo, L. Gu, D. Yi, X. R. Wang, H. Huang, J. L. MacManus-Driscoll, L.-Q. Chen, K.-J. Jin, C.-W. Nan, Y.-H. Lin, *Science* **2021**, *374*, 100.
- [83] J. Li, F. Li, Z. Xu, S. Zhang, *Adv. Mater.* **2018**, *30*, 1802155.
- [84] H. Qi, R. Zuo, A. Xie, A. Tian, J. Fu, Y. Zhang, S. Zhang, *Adv. Funct. Mater.* **2019**, *29*, 1903877.
- [85] T. Li, S. Deng, H. Liu, S. Sun, H. Li, S. Hu, S. Liu, X. Xing, J. Chen, *Adv. Mater.* **2021**, *33*, 2008316.
- [86] K. Huang, G. Ge, F. Yan, B. Shen, J. Zhai, *Adv. Electron. Mater.* **2020**, *6*, 1901366.
- [87] J. Gao, Q. Li, S. Zhang, J.-F. Li, *J. Appl. Phys.* **2020**, *128*, 070903.
- [88] K. Yamasaki, Y. Soejima, K. F. Fischer, *Acta Cryst. B* **1998**, *54*, 524.
- [89] K. Kobayashi, M. Ryu, Y. Doshida, Y. Mizuno, C. A. Randall, X. Tan, *J. Am. Ceram. Soc.* **2013**, *96*, 531.
- [90] A. K. Tagantsev, K. Vaideeswaran, S. B. Vakhruшев, A. V. Filimonov, R. G. Burkovsky, A. Shaganov, D. Andronikova, A. I. Rudskoy,

- A. Q. Baron, H. Uchiyama, D. Chernyshov, A. Bosak, Z. Ujma, K. Roleder, A. Majchrowski, J. H. Ko, N. Setter, *Nat. Commun.* **2013**, *4*, 2229.
- [91] J. Hlinka, T. Ostapchuk, E. Buixaderas, C. Kadlec, P. Kuzel, I. Gregora, J. Kroupa, M. Savinov, A. Klic, J. Drahokoupil, I. Etxebarria, J. Dec, *Phys. Rev. Lett.* **2014**, *112*, 197601.
- [92] B. Xu, O. Hellman, L. Bellaiche, *Phys. Rev. B* **2019**, *100*, 020102(R).
- [93] P. Yang, D. A. Payne, *J. Appl. Phys.* **1992**, *71*, 1361.
- [94] O. E. Fesenko, R. V. Kolesova, Y. G. Sindeyev, *Ferroelectrics* **1978**, *20*, 177.
- [95] H. Wang, Y. Liu, T. Yang, S. Zhang, *Adv. Funct. Mater.* **2019**, *29*, 1807321.
- [96] T. Zhang, Y. Zhao, W. Li, W. Fei, *Energy Storage Mater.* **2019**, *18*, 238.
- [97] X. Liu, Y. Li, N. Sun, X. Hao, *Inorg. Chem. Front.* **2020**, *7*, 756.
- [98] X.-K. Wei, C. L. Jia, H. C. Du, K. Roleder, J. Mayer, R. E. Dunin-Borkowski, *Adv. Mater.* **2020**, *32*, 1907208.
- [99] X.-K. Wei, C. L. Jia, K. Roleder, R. E. Dunin-Borkowski, J. Mayer, *Adv. Funct. Mater.* **2021**, *31*, 2008609.
- [100] X.-K. Wei, R. E. Dunin-Borkowski, J. Mayer, *Materials* **2021**, *14*, 7854.
- [101] T. H. Kim, D. Puggioni, Y. Yuan, L. Xie, H. Zhou, N. Campbell, P. J. Ryan, Y. Choi, J. W. Kim, J. R. Patzner, S. Ryu, J. P. Podkaminer, J. Irwin, Y. Ma, C. J. Fennie, M. S. Rzechowski, X. Q. Pan, V. Gopalan, J. M. Rondinelli, C. B. Eom, *Nature* **2016**, *533*, 68.
- [102] C. L. Jia, S. B. Mi, M. Faley, U. Poppe, J. Schubert, K. Urban, *Phys. Rev. B* **2009**, *79*, 081405.
- [103] J. M. Rondinelli, C. J. Fennie, *Adv. Mater.* **2012**, *24*, 1961.
- [104] X. Tan, C. Ma, J. Frederick, S. Beckman, K. G. Webber, *J. Am. Ceram. Soc.* **2011**, *94*, 4091.
- [105] D. Viehland, X. H. Dai, J. F. Li, Z. Xu, *J. Appl. Phys.* **1998**, *84*, 458.
- [106] T. Ma, Z. Fan, B. Xu, T.-H. Kim, P. Lu, L. Bellaiche, M. J. Kramer, X. Tan, L. Zhou, *Phys. Rev. Lett.* **2019**, *123*, 217602.
- [107] I. MacLaren, R. Villaurrutia, B. Schaffer, L. Houben, A. Peláiz-Barranco, *Adv. Funct. Mater.* **2012**, *22*, 261.
- [108] Z. Fu, X. Chen, Z. Li, T. Hu, L. Zhang, P. Lu, S. Zhang, G. Wang, X. Dong, F. Xu, *Nat. Commun.* **2020**, *11*, 3809.
- [109] H. Liu, Z. Zhou, Y. Qiu, B. Gao, S. Sun, K. Lin, L. Ding, Q. Li, Y. Cao, Y. Ren, J. Sun, X. Xing, J. Chen, *Mater. Horiz.* **2020**, *7*, 1912.
- [110] D. Berlincourt, H. H. A. Krueger, B. Jaffe, *J. Phys. Chem. Solids* **1964**, *25*, 659.
- [111] F. El-Mellouhi, E. N. Brothers, M. J. Lucero, G. E. Scuseria, *Phys. Rev. B* **2011**, *84*, 115122.
- [112] P. Noel, F. Trier, L. M. Vicente Arche, J. Brehin, D. C. Vaz, V. Garcia, S. Fusil, A. Barthelemy, L. Vila, M. Bibes, J. P. Attane, *Nature* **2020**, *580*, 483.
- [113] Y. Tomioka, N. Shirakawa, K. Shibuya, I. H. Inoue, *Nat. Commun.* **2019**, *10*, 738.
- [114] Y. Frenkel, N. Haham, Y. Shperber, C. Bell, Y. Xie, Z. Chen, Y. Hikita, H. Y. Hwang, E. K. H. Salje, B. Kalisky, *Nat. Mater.* **2017**, *16*, 1203.
- [115] H. E. Weaver, *J. Phys. Chem. Solids* **1959**, *11*, 274.
- [116] R. Xu, J. Huang, E. S. Barnard, S. S. Hong, P. Singh, E. K. Wong, T. Jansen, V. Harbola, J. Xiao, B. Y. Wang, S. Crossley, D. Lu, S. Liu, H. Y. Hwang, *Nat. Commun.* **2020**, *11*, 3141.
- [117] J. H. Haeni, P. Irvin, W. Chang, R. Uecker, P. Reiche, Y. L. Li, S. Choudhury, W. Tian, M. E. Hawley, B. Craigo, A. K. Tagantsev, X. Q. Pan, S. K. Streiffer, L. Q. Chen, S. W. Kirchoefer, J. Levy, D. G. Schlom, *Nature* **2004**, *430*, 758.
- [118] T. F. Nova, A. S. Disa, M. Fechner, A. Cavalleri, *Science* **2019**, *364*, 1075.
- [119] X. Li, T. Qiu, J. Zhang, E. Baldini, J. Lu, A. M. Rappe, K. A. Nelson, *Science* **2019**, *364*, 1079.
- [120] A. Kvasov, A. K. Tagantsev, N. Setter, *Phys. Rev. B* **2016**, *94*, 054102.
- [121] L. Arzel, B. Hehlen, A. K. Tagantsev, F. Denoyer, K. D. Liss, R. Currat, E. Courtens, *Ferroelectrics* **2002**, *267*, 317.
- [122] S. Salmani-Rezaie, K. Ahadi, W. M. Strickland, S. Stemmer, *Phys. Rev. Lett.* **2020**, *125*, 087601.
- [123] R. Blinc, B. Zalar, V. V. Laguta, M. Itoh, *Phys. Rev. Lett.* **2005**, *94*, 147601.
- [124] H. W. Jang, A. Kumar, S. Denev, M. D. Biegalski, P. Maksymovych, C. W. Bark, C. T. Nelson, C. M. Folkman, S. H. Baek, N. Balke, C. M. Brooks, D. A. Tenne, D. G. Schlom, L. Q. Chen, X. Q. Pan, S. V. Kalinin, V. Gopalan, C. B. Eom, *Phys. Rev. Lett.* **2010**, *104*, 197601.
- [125] B. Peng, Q. Zhang, X. Li, T. Sun, H. Fan, S. Ke, M. Ye, Y. Wang, W. Lu, H. Niu, J. F. Scott, X. Zeng, H. Huang, *Adv. Electron. Mater.* **2015**, *1*, 1500052.
- [126] P. Nukala, M. Ahmadi, Y. Wei, S. d. Graaf, E. Stylianidis, T. Chakraborty, S. Matzen, H. W. Zandbergen, A. Björling, D. Mannix, D. Carbone, B. Kooi, B. Noheda, *Science* **2021**, *372*, 630.
- [127] L. Yao, S. Inkinen, S. van Dijken, *Nat. Commun.* **2017**, *8*, 14544.
- [128] M. Höfling, X. Zhou, L. M. Riemer, E. Bruder, B. Liu, L. Zhou, P. B. Groszewicz, F. Zhuo, B.-X. Xu, K. Durst, X. Tan, D. Damjanovic, J. Koruza, J. Röde, *Science* **2021**, *372*, 961.
- [129] Y. Saito, H. Takao, T. Tani, T. Nonoyama, K. Takatori, T. Homma, T. Nagaya, M. Nakamura, *Nature* **2004**, *432*, 84.
- [130] E. Birks, M. Dunce, R. Ignatans, A. Kuzmin, A. Plaude, M. Antonova, K. Kundzins, A. Sternberg, *J. Appl. Phys.* **2016**, *119*, 074102.
- [131] Y. Liu, Y. Ji, Y. Yang, *Nanomaterials* **2021**, *11*, 1724.
- [132] K. Watanabe, Y. Iikubo, Y. Yamaguchi, A. Kudo, *Chem. Commun.* **2021**, *57*, 323.
- [133] G. A. Smolenskii, V. A. Isupov, A. I. Agranovskaya, N. N. Krainik, *Sov. Phys. Solid State* **1961**, *2*, 2651.
- [134] S. Gorfman, P. A. Thomas, *J. Appl. Crystallogr.* **2010**, *43*, 1409.
- [135] B. N. Rao, A. N. Fitch, R. Ranjan, *Phys. Rev. B* **2013**, *87*, 060102.
- [136] B. N. Rao, L. Olivi, V. Sathe, R. Ranjan, *Phys. Rev. B* **2016**, *93*, 024102.
- [137] G. Das Adhikary, B. Mahale, B. N. Rao, A. Senyshyn, R. Ranjan, *Phys. Rev. B* **2021**, *103*, 184106.
- [138] T. Takenaka, K.-i. Maruyama, K. Sakata, *Jpn. J. Appl. Phys.* **1991**, *30*, 2236.
- [139] F. Cordero, F. Craciun, F. Trequattrini, E. Mercadelli, C. Galassi, *Phys. Rev. B* **2010**, *81*, 144124.
- [140] K. Datta, R. B. Neder, A. Richter, M. Göbbels, J. C. Neufeind, B. Mihailova, *Phys. Rev. B* **2018**, *97*, 184101.
- [141] J. Yin, H. Zong, H. Tao, X. Tao, H. Wu, Y. Zhang, L.-D. Zhao, X. Ding, J. Sun, J. Zhu, J. Wu, S. J. Pennycook, *Nat. Commun.* **2021**, *12*, 3632.
- [142] J. Song, J. Gao, S. Zhang, L. Luo, X. Dai, L. Zhao, B. Liu, *Crystals* **2019**, *9*, 558.
- [143] C. Yang, P. Lv, J. Qian, Y. Han, J. Ouyang, X. Lin, S. Huang, Z. Cheng, *Adv. Energy Mater.* **2019**, *9*, 1803949.
- [144] J. Li, Z. Shen, X. Chen, S. Yang, W. Zhou, M. Wang, L. Wang, Q. Kou, Y. Liu, Q. Li, Z. Xu, Y. Chang, S. Zhang, F. Li, *Nat. Mater.* **2020**, *19*, 999.
- [145] M. Wang, Q. Feng, C. Luo, Y. Lan, C. Yuan, N. Luo, C. Zhou, T. Fujita, J. Xu, G. Chen, Y. Wei, *ACS Appl. Mater. Interfaces* **2021**, *13*, 51218.
- [146] R. Bhattacharyya, S. Das, S. Omar, *Acta Mater.* **2018**, *159*, 8.
- [147] J. Ma, J. Ma, Q. Zhang, R. Peng, J. Wang, C. Liu, M. Wang, N. Li, M. Chen, X. Cheng, P. Gao, L. Gu, L. Q. Chen, P. Yu, J. Zhang, C. W. Nan, *Nat. Nanotechnol.* **2018**, *13*, 947.
- [148] W. Yang, G. Tian, Y. Zhang, F. Xue, D. Zheng, L. Zhang, Y. Wang, C. Chen, Z. Fan, Z. Hou, D. Chen, J. Gao, M. Zeng, M. Qin, L. Q. Chen, X. Gao, J. M. Liu, *Nat. Commun.* **2021**, *12*, 1306.
- [149] M. Stengel, N. A. Spaldin, *Nature* **2006**, *443*, 679.
- [150] M. Stengel, D. Vanderbilt, N. A. Spaldin, *Nat. Mater.* **2009**, *8*, 392.
- [151] X.-K. Wei, Y. Yang, L. J. McCilly, L. Feigl, R. E. Dunin-Borkowski, C.-L. Jia, L. Bellaiche, N. Setter, *Phys. Rev. B* **2018**, *98*, 020102(R).
- [152] I. Massiot, A. Cattoni, S. Collin, *Nat. Energy* **2020**, *5*, 959.
- [153] N.-G. Park, K. Zhu, *Nat. Rev. Mater.* **2020**, *5*, 333.
- [154] A. K. Jena, A. Kulkarni, T. Miyasaka, *Chem. Rev.* **2019**, *119*, 3036.

- [155] Y. Yuan, T. J. Reece, P. Sharma, S. Poddar, S. Ducharme, A. Gruverman, Y. Yang, J. Huang, *Nat. Mater.* **2011**, *10*, 296.
- [156] S. Y. Yang, J. Seidel, S. J. Byrnes, P. Shafer, C. H. Yang, M. D. Rossell, P. Yu, Y. H. Chu, J. F. Scott, J. W. Ager, L. W. Martin, R. Ramesh, *Nat. Nanotechnol.* **2010**, *5*, 143.
- [157] J. E. Spanier, V. M. Fridkin, A. M. Rappe, A. R. Akbashev, A. Polemi, Y. Qi, Z. Gu, S. M. Young, C. J. Hawley, D. Imbrenda, G. Xiao, A. L. Bennett-Jackson, C. L. Johnson, *Nat. Photonics* **2016**, *10*, 611.
- [158] A. Kojima, K. Teshima, Y. Shirai, T. Miyasaka, *J. Am. Ceram. Soc.* **2009**, *131*, 6050.
- [159] B. Vargas, G. Rodríguez-López, D. Solis-Ibarra, *ACS Energy Lett.* **2020**, *5*, 3591.
- [160] B. Huang, Z. Liu, C. Wu, Y. Zhang, J. Zhao, X. Wang, J. Li, *Natl. Sci. Rev.* **2021**, *8*, nwab094.
- [161] J. Jeong, M. Kim, J. Seo, H. Lu, P. Ahlawat, A. Mishra, Y. Yang, M. A. Hope, F. T. Eickemeyer, M. Kim, Y. J. Yoon, I. W. Choi, B. P. Darwich, S. J. Choi, Y. Jo, J. H. Lee, B. Walker, S. M. Zakeeruddin, L. Emsley, U. Rothlisberger, A. Hagfeldt, D. S. Kim, M. Gratzel, J. Y. Kim, *Nature* **2021**, *592*, 381.
- [162] Y. Zhao, T. Heumueller, J. Zhang, J. Luo, O. Kasian, S. Langner, C. Kupfer, B. Liu, Y. Zhong, J. Elia, A. Osvet, J. Wu, C. Liu, Z. Wan, C. Jia, N. Li, J. Hauch, C. J. Brabec, *Nat. Energy* **2021**, *7*, 144.
- [163] B. Guzelturk, R. A. Belisle, M. D. Smith, K. Bruening, R. Prasanna, Y. Yuan, V. Gopalan, C. J. Tassone, H. I. Karunadasa, M. D. McGehee, A. M. Lindenberg, *Adv. Mater.* **2018**, *30*, 1704737.
- [164] X. T. Wu, L. Z. Tan, X. Shen, T. Hu, K. Miyata, M. T. Trinh, R. C. Li, S. Liu, D. A. Egger, I. Makasyuk, Q. Zheng, A. Fry, J. S. Robinson, M. D. Smith, B. Guzelturk, H. I. Karunadasa, X. Wang, X. Zhu, L. Kronik, A. M. Rappe, A. M. Lindenberg, *Sci. Adv.* **2017**, *3*, e1602388.
- [165] A. J. Neukirch, W. Nie, J. C. Blancon, K. Appavoo, H. Tsai, M. Y. Sfeir, C. Katan, L. Pedesseau, J. Even, J. J. Crochet, G. Gupta, A. D. Mohite, S. Tretiak, *Nano Lett.* **2016**, *16*, 3809.
- [166] K. Miyata, D. Meggiolaro, M. T. Trinh, P. P. Joshi, E. Mosconi, S. C. Jones, F. de Angelis, X. Y. Zhu, *Sci. Adv.* **2017**, *3*, e1701217.
- [167] J. M. Frost, K. T. Butler, F. Brivio, C. H. Hendon, M. van Schilfegaarde, A. Walsh, *Nano Lett.* **2014**, *14*, 2584.
- [168] S. Shahrokhi, W. Gao, Y. Wang, P. R. Anandan, M. Z. Rahaman, S. Singh, D. Wang, C. Cazorla, G. Yuan, J. M. Liu, T. Wu, *Small Methods* **2020**, *4*, 2000149.
- [169] H. Zarenezhad, M. Askari, M. Halali, N. Solati, T. Balkan, S. Kaya, *Sol. Energy Mater. Sol. Cells* **2020**, *206*, 110318.
- [170] A. Poglitsch, D. Weber, *J. Chem. Phys.* **1987**, *87*, 6373.
- [171] Y. Dang, Y. Liu, Y. Sun, D. Yuan, X. Liu, W. Lu, G. Liu, H. Xia, X. Tao, *CrystEngComm* **2015**, *17*, 665.
- [172] H. Rohm, T. Leonhard, A. D. Schulz, S. Wagner, M. J. Hoffmann, A. Colsmann, *Adv. Mater.* **2019**, *31*, 1806661.
- [173] L. M. Garten, D. T. Moore, S. U. Nanayakkara, S. Dwaraknath, P. Schulz, J. Wands, A. Rockett, B. Newell, K. A. Persson, S. Trolrier-McKinstry, D. S. Ginley, *Sci. Adv.* **2019**, *5*, eaas9311.
- [174] M. Coll, A. Gomez, E. Mas-Marza, O. Almora, G. Garcia-Belmonte, M. Campoy-Quiles, J. Bisquert, *J. Phys. Chem. Lett.* **2015**, *6*, 1408.
- [175] J. Breternitz, F. Lehmann, S. A. Barnett, H. Nowell, S. Schorr, *Angew. Chem., Int. Ed.* **2020**, *59*, 424.
- [176] D. B. Straus, S. Guo, A. M. Abeykoon, R. J. Cava, *Adv. Mater.* **2020**, *32*, 2001069.
- [177] H. Wei, Y. Yang, S. Chen, H. J. Xiang, *Nat. Commun.* **2021**, *12*, 637.
- [178] V. C. A. Taylor, D. Tiwari, M. Duchi, P. M. Donaldson, I. P. Clark, D. J. Fermin, T. A. A. Oliver, *J. Phys. Chem. Lett.* **2018**, *9*, 895.
- [179] O. Yaffe, Y. Guo, L. Z. Tan, D. A. Egger, T. Hull, C. C. Stoumpos, F. Zheng, T. F. Heinz, L. Kronik, M. G. Kanatzidis, J. S. Owen, A. M. Rappe, M. A. Pimenta, L. E. Brus, *Phys. Rev. Lett.* **2017**, *118*, 136001.
- [180] A. N. Beecher, O. E. Semonin, J. M. Skelton, J. M. Frost, M. W. Terban, H. Zhai, A. Alatas, J. S. Owen, A. Walsh, S. J. L. Billinge, *ACS Energy Lett.* **2016**, *1*, 880.
- [181] Y. Yang, F. Lou, H. Xiang, *Nano Lett.* **2021**, *21*, 3170.
- [182] W. Q. Liao, Y. Zhang, C. L. Hu, J. G. Mao, H. Y. Ye, P. F. Li, S. D. Huang, R. G. Xiong, *Nat. Commun.* **2015**, *6*, 7338.
- [183] H. Tsai, W. Nie, J. C. Blancon, C. C. Stoumpos, R. Asadpour, B. Harutyunyan, A. J. Neukirch, R. Verduzco, J. J. Crochet, S. Tretiak, L. Pedesseau, J. Even, M. A. Alam, G. Gupta, J. Lou, P. M. Ajayan, M. J. Bedzyk, M. G. Kanatzidis, *Nature* **2016**, *536*, 312.
- [184] Y. Huang, Y. Li, E. L. Lim, T. Kong, Y. Zhang, J. Song, A. Hagfeldt, D. Bi, *J. Am. Chem. Soc.* **2021**, *143*, 3911.
- [185] L. Etgar, *Energy Environ. Sci.* **2018**, *11*, 234.
- [186] X. Liu, A. Chanana, U. Huynh, F. Xue, P. Haney, S. Blair, X. Jiang, Z. V. Vardeny, *Nat. Commun.* **2020**, *11*, 323.
- [187] Y. Zhai, S. Baniya, C. Zhang, J. Li, P. Haney, C.-X. Sheng, E. Ehrenfreund, Z. V. Vardeny, *Sci. Adv.* **2017**, *3*, e1700704.
- [188] M. T. Pham, E. Amerling, H. M. Luong, H. T. Pham, G. K. Larsen, L. Whittaker-Brooks, T. D. Nguyen, *Sci. Rep.* **2020**, *10*, 4964.
- [189] K. Frohna, T. Deshpande, J. Harter, W. Peng, B. A. Barker, J. B. Neaton, S. G. Louie, O. M. Bakr, D. Hsieh, M. Bernardi, *Nat. Commun.* **2018**, *9*, 1829.
- [190] F. Zheng, L. Z. Tan, S. Liu, A. M. Rappe, *Nano Lett.* **2015**, *15*, 7794.
- [191] K. X. Jin, Y. F. Li, Z. L. Wang, H. Y. Peng, W. N. Lin, A. K. K. Kyaw, Y. L. Jin, K. J. Jin, X. W. Sun, C. Soci, T. Wu, *AIP Adv.* **2012**, *2*, 042131.
- [192] X. L. Xu, L. B. Xiao, J. Zhao, B. K. Pan, J. Li, W. Q. Liao, R. G. Xiong, G. F. Zou, *Angew. Chem., Int. Ed.* **2020**, *59*, 19974.
- [193] T. T. Sha, Y. A. Xiong, Q. Pan, X. G. Chen, X. J. Song, J. Yao, S. R. Miao, Z. Y. Jing, Z. J. Feng, Y. M. You, R. G. Xiong, *Adv. Mater.* **2019**, *31*, 1901843.
- [194] C.-R. Huang, X. Luo, X.-G. Chen, X.-J. Song, Z.-X. Zhang, R.-G. Xiong, *Natl. Sci. Rev.* **2021**, *8*, nwaa232.
- [195] Y. Hou, C. Wu, D. Yang, T. Ye, V. G. Honavar, A. C. T. van Duin, K. Wang, S. Priya, *J. Appl. Phys.* **2020**, *128*, 060906.
- [196] T. Akamatsu, T. Ideue, L. Zhou, Y. Dong, S. Kitamura, M. Yoshii, D. Yang, M. Onga, Y. Nakagawa, K. Watanabe, T. Taniguchi, J. Laurienzo, J. Huang, Z. Ye, T. Morimoto, H. Yuan, Y. Iwasa, *Science* **2021**, *372*, 68.
- [197] N. A. Pertsev, A. G. Zembilgotov, A. K. Tagantsev, *Phys. Rev. Lett.* **1998**, *80*, 1988.
- [198] J. Junquera, P. Ghosez, *Nature* **2003**, *422*, 506.
- [199] Y. Watanabe, *Phys. Rev. B* **1998**, *57*, 789.
- [200] I. I. Naumov, L. Bellaiche, H. Fu, *Nature* **2004**, *432*, 737.
- [201] L. Qi, S. Ruan, Y. J. Zeng, *Adv. Mater.* **2021**, *33*, 2005098.
- [202] L. Ju, J. Shang, X. Tang, L. Kou, *J. Am. Chem. Soc.* **2020**, *142*, 1492.
- [203] C. Cui, F. Xue, W.-J. Hu, L.-J. Li, *Npj 2D Mater. Appl.* **2018**, *2*, 18.
- [204] J. H. Choi, S. H. Jhi, *J. Phys. Condens. Matter* **2020**, *32*, 045702.
- [205] Q. Peng, D. Li, P. Huang, Y. Ren, Z. Li, L. Pi, P. Chen, M. Wu, X. Zhang, X. Zhou, T. Zhai, *ACS Nano* **2021**, *15*, 16525.
- [206] V. Maisonneuve, V. Cajipe, A. Simon, R. Von Der Muhll, J. Ravez, *Phys. Rev. B* **1997**, *56*, 10860.
- [207] M. Si, P. Y. Liao, G. Qiu, Y. Duan, P. D. Ye, *ACS Nano* **2018**, *12*, 6700.
- [208] P. Yu, F. Wang, J. Meng, T. A. Shifa, M. G. Sendeku, J. Fang, S. Li, Z. Cheng, X. Lou, J. He, *CrystEngComm* **2021**, *23*, 591.
- [209] F. Liu, L. You, K. L. Seyler, X. Li, P. Yu, J. Lin, X. Wang, J. Zhou, H. Wang, H. He, S. T. Pantelides, W. Zhou, P. Sharma, X. Xu, P. M. Ajayan, J. Wang, Z. Liu, *Nat. Commun.* **2016**, *7*, 12357.
- [210] J. A. Brehm, S. M. Neumayer, L. Tao, A. O'Hara, M. Chyasnovich, M. A. Susner, M. A. McGuire, S. V. Kalinin, S. Jesse, P. Ganesh, S. T. Pantelides, P. Maksymovych, N. Balke, *Nat. Mater.* **2020**, *19*, 43.
- [211] I. Katsouras, K. Asadi, M. Li, T. B. van Driel, K. S. Kjaer, D. Zhao, T. Lenz, Y. Gu, P. W. Blom, D. Damjanovic, M. M. Nielsen, D. M. de Leeuw, *Nat. Mater.* **2016**, *15*, 78.
- [212] L. You, Y. Zhang, S. Zhou, A. Chaturvedi, S. A. Morris, F. Liu, L. Chang, D. Ichinose, I. Funakubo, W. Hu, T. Wu, Z. Liu, S. Dong, J. Wang, *Sci. Adv.* **2019**, *5*, eaav3780.
- [213] V. Maisonneuve, J. M. Reau, M. Dong, V. B. Cajipe, C. Payen, J. Ravez, *Ferroelectrics* **1997**, *196*, 257.

- [214] S. M. Neumayer, L. Tao, A. O'Hara, J. Brehm, M. Si, P.-Y. Liao, T. Feng, S. V. Kalinin, P. D. Ye, S. T. Pantelides, P. Maksymovych, N. Balke, *Phys. Rev. Appl.* **2020**, *13*, 064063.
- [215] D. Zhang, Z. D. Luo, Y. Yao, P. Schoenherr, C. Sha, Y. Pan, P. Sharma, M. Alexe, J. Seidel, *Nano Lett.* **2021**, *21*, 995.
- [216] Y. Li, J. Fu, X. Mao, C. Chen, H. Liu, M. Gong, H. Zeng, *Nat. Commun.* **2021**, *12*, 5896.
- [217] S. Zhou, L. You, H. Zhou, Y. Pu, Z. Gui, J. Wang, *Front. Phys.* **2020**, *16*, 13301.
- [218] D. D. Xu, R. R. Ma, A. P. Fu, Z. Guan, N. Zhong, H. Peng, P. H. Xiang, C. G. Duan, *Nat. Commun.* **2021**, *12*, 655.
- [219] S. M. Yang, A. N. Morozovska, R. Kumar, E. A. Eliseev, Y. Cao, L. Mazet, N. Balke, S. Jesse, R. K. Vasudevan, C. Dubourdieu, S. V. Kalinin, *Nat. Phys.* **2017**, *13*, 812.
- [220] A. N. Morozovska, E. A. Eliseev, N. V. Morozovsky, S. V. Kalinin, *Phys. Rev. B* **2017**, *95*, 195413.
- [221] Y. Fan, X. Song, H. Ai, W. Li, M. Zhao, *ACS Appl. Mater. Interfaces* **2021**, *13*, 34486.
- [222] L. Niu, F. Liu, Q. Zeng, X. Zhu, Y. Wang, P. Yu, J. Shi, J. Lin, J. Zhou, Q. Fu, W. Zhou, T. Yu, X. Liu, Z. Liu, *Nano Energy* **2019**, *58*, 596.
- [223] Z. Yang, J. Zhang, M. C. Kintner-Meyer, X. Lu, D. Choi, J. P. Lemmon, J. Liu, *Chem. Rev.* **2011**, *111*, 3577.
- [224] T. Lan, C.-L. Tsai, F. Tietz, X.-K. Wei, M. Heggen, R. E. Dunin-Borkowski, R. Wang, Y. Xiao, Q. Ma, O. Guillon, *Nano Energy* **2019**, *65*, 104040.
- [225] J. Li, R. Guttinger, R. More, F. Song, W. Wan, G. R. Patzke, *Chem. Soc. Rev.* **2017**, *46*, 6124.
- [226] S. Nitopi, E. Bertheussen, S. B. Scott, X. Liu, A. K. Engstfeld, S. Horch, B. Seger, I. E. L. Stephens, K. Chan, C. Hahn, J. K. Nørskov, T. F. Jaramillo, I. Chorkendorff, *Chem. Rev.* **2019**, *119*, 7610.
- [227] X. Zhang, S.-X. Guo, K. A. Gandionco, A. M. Bond, J. Zhang, *Mater. Today Adv.* **2020**, *7*, 100074.
- [228] S. Tu, Y. Guo, Y. Zhang, C. Hu, T. Zhang, T. Ma, H. Huang, *Adv. Funct. Mater.* **2020**, *30*, 2005158.
- [229] Y. J. Chung, C. S. Yang, J. T. Lee, G. H. Wu, J. M. Wu, *Adv. Energy Mater.* **2020**, *10*, 2002082.
- [230] J. Wang, *Analytical Electrochemistry*, Wiley, Hoboken, NJ **2006**, pp. 1–28.
- [231] A. J. Bard, L. R. Faulkner, *Electrochemical Methods Fundamentals and Applications*, 2nd ed., Wiley, New York **2001**.
- [232] A. Vojvodic, J. K. Nørskov, *Natl. Sci. Rev.* **2015**, *2*, 140.
- [233] X. Zou, Y. Zhang, *Chem. Soc. Rev.* **2015**, *44*, 5148.
- [234] J. Li, M. Hong, L. Sun, W. Zhang, H. Shu, H. Chang, *ACS Appl. Mater. Interfaces* **2018**, *10*, 458.
- [235] X. Wang, J. Wang, B. Wei, N. Zhang, J. Xu, H. Miao, L. Liu, C. Su, Y. Li, Z. Wang, *J. Mater. Sci. Technol.* **2021**, *78*, 170.
- [236] H. Wang, X. Qian, *Npj Comput. Mater.* **2019**, *5*, 119.
- [237] B. Zhao, B. Karpiak, D. Khokhriakov, A. Johansson, A. M. Hoque, X. Xu, Y. Jiang, I. Mertig, S. P. Dash, *Adv. Mater.* **2020**, *32*, 2000818.
- [238] Q. Wang, J. Li, J. Besbas, C. H. Hsu, K. Cai, L. Yang, S. Cheng, Y. Wu, W. Zhang, K. Wang, T. R. Chang, H. Lin, H. Chang, H. Yang, *Adv. Sci.* **2018**, *5*, 1700912.
- [239] P. Li, Y. Wen, X. He, Q. Zhang, C. Xia, Z. M. Yu, S. A. Yang, Z. Zhu, H. N. Alshareef, X. X. Zhang, *Nat. Commun.* **2017**, *8*, 2150.
- [240] F. T. Huang, S. Joon Lim, S. Singh, J. Kim, L. Zhang, J. W. Kim, M. W. Chu, K. M. Rabe, D. Vanderbilt, S. W. Cheong, *Nat. Commun.* **2019**, *10*, 4211.
- [241] K. Deng, G. Wan, P. Deng, K. Zhang, S. Ding, E. Wang, M. Yan, H. Huang, H. Zhang, Z. Xu, J. Denlinger, A. Fedorov, H. Yang, W. Duan, H. Yao, Y. Wu, S. Fan, H. Zhang, X. Chen, S. Zhou, *Nat. Phys.* **2016**, *12*, 1105.
- [242] T. Sluka, A. K. Tagantsev, D. Damjanovic, M. Gureev, N. Setter, *Nat. Commun.* **2012**, *3*, 748.
- [243] T. Sluka, A. K. Tagantsev, P. Bednyakov, N. Setter, *Nat. Commun.* **2013**, *4*, 1808.
- [244] A. Crassous, T. Sluka, A. K. Tagantsev, N. Setter, *Nat. Nanotechnol.* **2015**, *10*, 614.
- [245] N. A. Benedek, T. Birol, *J. Mater. Chem. C* **2016**, *4*, 4000.
- [246] D. Puggioni, J. M. Rondinelli, *Nat. Commun.* **2014**, *5*, 3432.
- [247] Q. Yang, M. Wu, J. Li, *J. Phys. Chem. Lett.* **2018**, *9*, 7160.
- [248] Z. Fei, W. Zhao, T. A. Palomaki, B. Sun, M. K. Miller, Z. Zhao, J. Yan, X. Xu, D. H. Cobden, *Nature* **2018**, *560*, 336.
- [249] S. C. de la Barrera, Q. Cao, Y. Gao, Y. Gao, V. S. Bheemarasetty, J. Yan, D. G. Mandrus, W. Zhu, D. Xiao, B. M. Hunt, *Nat. Commun.* **2021**, *12*, 5298.
- [250] P. Sharma, F.-X. Xiang, D.-F. Shao, D. Zhang, E. Y. Tsymbal, A. R. Hamilton, J. Seidel, *Sci. Adv.* **2019**, *5*, eaax5080.
- [251] X. Geng, W. Sun, W. Wu, B. Chen, A. Al-Hilo, M. Benamara, H. Zhu, F. Watanabe, J. Cui, T. P. Chen, *Nat. Commun.* **2016**, *7*, 10672.
- [252] J. C. McGlynn, T. Dankwort, L. Kienle, N. A. G. Bandeira, J. P. Fraser, E. K. Gibson, I. Cascallana-Matias, K. Kamaras, M. D. Symes, H. N. Miras, A. Y. Ganin, *Nat. Commun.* **2019**, *10*, 4916.
- [253] B. Zhao, D. Khokhriakov, Y. Zhang, H. Fu, B. Karpiak, A. M. Hoque, X. Xu, Y. Jiang, B. Yan, S. P. Dash, *Phys. Rev. Res.* **2020**, *2*, 013286.
- [254] C. Ke, J. Huang, S. Liu, *Mater. Horiz.* **2021**, *8*, 3387.
- [255] B. E. Hayden, *Acc. Chem. Res.* **2013**, *46*, 1858.
- [256] C. Y. Li, J. B. Le, Y. H. Wang, S. Chen, Z. L. Yang, J. F. Li, J. Cheng, Z. Q. Tian, *Nat. Mater.* **2019**, *18*, 697.
- [257] Y. H. Wang, S. Zheng, W. M. Yang, R. Y. Zhou, Q. F. He, P. Radjenovic, J. C. Dong, S. Li, J. Zheng, Z. L. Yang, G. Attard, F. Pan, Z. Q. Tian, J. F. Li, *Nature* **2021**, *600*, 81.
- [258] J. T. Mefford, A. R. Akbashev, M. Kang, C. L. Bentley, W. E. Gent, H. D. Deng, D. H. Alsem, Y. S. Yu, N. J. Salmon, D. A. Shapiro, P. R. Unwin, W. C. Chueh, *Nature* **2021**, *593*, 67.
- [259] Y. P. Zhu, C. Guo, Y. Zheng, S. Z. Qiao, *Acc. Chem. Res.* **2017**, *50*, 915.
- [260] A. B. Laursen, K. R. Patraju, M. J. Whitaker, M. Retuerto, T. Sarkar, N. Yao, K. V. Ramanujachary, M. Greenblatt, G. C. Dismukes, *Energy Environ. Sci.* **2015**, *8*, 1027.
- [261] J. Kibsgaard, C. Tsai, K. Chan, J. D. Benck, J. K. Nørskov, F. Abild-Pedersen, T. F. Jaramillo, *Energy Environ. Sci.* **2015**, *8*, 3022.
- [262] E. J. Popczun, J. R. McKone, C. G. Read, A. J. Biacchi, A. M. Wiltrout, N. S. Lewis, R. E. Schaak, *J. Am. Chem. Soc.* **2013**, *135*, 9267.
- [263] L.-A. Stern, L. Feng, F. Song, X. Hu, *Energy Environ. Sci.* **2015**, *8*, 2347.
- [264] K. U. D. Calvino, A. B. Laursen, K. M. K. Yap, T. A. Goetjen, S. Hwang, N. Murali, B. Mejia-Sosa, A. Lubarski, K. M. Teeluck, E. S. Hall, E. Garfunkel, M. Greenblatt, G. C. Dismukes, *Energy Environ. Sci.* **2018**, *11*, 2550.
- [265] J. A. Rodriguez, J.-Y. Kim, J. C. Hanson, S. J. Sawhill, M. E. Bussell, *J. Phys. Chem. B* **2003**, *107*, 6267.
- [266] X.-K. Wei, G. Bihlmayer, X. Zhou, W. Feng, Y. V. Kolen'ko, D. Xiong, L. Liu, S. Blugel, R. E. Dunin-Borkowski, *Adv. Mater.* **2020**, *32*, 2003479.
- [267] S. Anantharaj, S. R. Ede, K. Sakthikumar, K. Karthick, S. Mishra, S. Kundu, *ACS Catal.* **2016**, *6*, 8069.
- [268] D. E. Schipper, Z. Zhao, H. Thirumalai, A. P. Leitner, S. L. Donaldson, A. Kumar, F. Qin, Z. Wang, L. C. Grabow, J. Bao, K. H. Whitmire, *Chem. Mater.* **2018**, *30*, 3588.
- [269] C. Yang, M. Y. Gao, Q. B. Zhang, J. R. Zeng, X. T. Li, A. P. Abbott, *Nano Energy* **2017**, *36*, 85.
- [270] J. Xu, X.-K. Wei, J. D. Costa, J. L. Lado, B. Owens-Baird, L. P. L. Gonçalves, S. P. S. Fernandes, M. Heggen, D. Y. Petrovykh, R. E. Dunin-Borkowski, K. Kovnir, Y. V. Kolen'ko, *ACS Catal.* **2017**, *7*, 5450.
- [271] H. Zhou, F. Yu, J. Sun, R. He, S. Chen, C. W. Chu, Z. Ren, *Proc. Natl. Acad. Sci. U. S. A.* **2017**, *114*, 5607.
- [272] J. Suntivich, K. J. May, H. A. Gasteiger, J. B. Goodenough, Y. Shao-Horn, *Science* **2011**, *334*, 1383.
- [273] F. A. Garcés-Pineda, M. Blasco-Ahicart, D. Nieto-Castro, N. López, J. R. Galán-Mascarós, *Nat. Energy* **2019**, *4*, 519.

- [274] X. Ren, T. Wu, Y. Sun, Y. Li, G. Xian, X. Liu, C. Shen, J. Gracia, H. J. Gao, H. Yang, Z. J. Xu, *Nat. Commun.* **2021**, *12*, 2608.
- [275] Y. Sun, S. Sun, H. Yang, S. Xi, J. Gracia, Z. J. Xu, *Adv. Mater.* **2020**, *32*, 2003297.
- [276] S. Rundqvist, *Acta Chem. Scand.* **1962**, *16*, 992.
- [277] Z. Lan, D. R. Småbråten, C. Xiao, T. Vegge, U. Aschauer, I. E. Castelli, *ACS Catal.* **2021**, *11*, 12692.
- [278] I. C. Man, H. Y. Su, F. Calle-Vallejo, H. A. Hansen, J. I. Martínez, N. G. Inoglu, J. Kitchin, T. F. Jaramillo, J. K. Nørskov, J. Rossmeisl, *ChemCatChem* **2011**, *3*, 1159.
- [279] R. Mankowsky, A. von Hoegen, M. Forst, A. Cavalleri, *Phys. Rev. Lett.* **2017**, *118*, 197601.
- [280] R. Su, H. A. Hsain, M. Wu, D. Zhang, X. Hu, Z. Wang, X. Wang, F. T. Li, X. Chen, L. Zhu, Y. Yang, Y. Yang, X. Lou, S. J. Pennycook, *Angew. Chem., Int. Ed.* **2019**, *58*, 15076.
- [281] N. Domingo, I. Gaponenko, K. Cordero-Edwards, N. Stucki, V. Perez-Dieste, C. Escudero, E. Pach, A. Verdaguier, P. Paruch, *Nanoscale* **2019**, *11*, 17920.
- [282] K. Cordero-Edwards, L. Rodríguez, A. Calò, M. J. Esplandiù, V. Pérez-Dieste, C. Escudero, N. Domingo, A. Verdaguier, *J. Phys. Chem. C* **2016**, *120*, 24048.
- [283] N. Domingo, E. Pach, K. Cordero-Edwards, V. Perez-Dieste, C. Escudero, A. Verdaguier, *Phys. Chem. Chem. Phys.* **2019**, *21*, 4920.
- [284] Y. Yun, E. I. Altman, *J. Am. Chem. Soc.* **2007**, *129*, 15684.
- [285] M. A. Khan, M. A. Nadeem, H. Idriss, *Surf. Sci. Rep.* **2016**, *71*, 1.
- [286] N. D. Mermin, *Rev. Mod. Phys.* **1979**, *51*, 591.
- [287] I. Roger, M. A. Shipman, M. D. Symes, *Nat. Rev. Chem.* **2017**, *1*, 0003.
- [288] T. Haas, R. Krause, R. Weber, M. Demler, G. Schmid, *Nat. Catal.* **2018**, *1*, 32.
- [289] L. Han, S. Song, M. Liu, S. Yao, Z. Liang, H. Cheng, Z. Ren, W. Liu, R. Lin, G. Qi, X. Liu, Q. Wu, J. Luo, H. L. Xin, *J. Am. Chem. Soc.* **2020**, *142*, 12563.
- [290] S. Tu, Y. Zhang, A. H. Reshak, S. Auluck, L. Ye, X. Han, T. Ma, H. Huang, *Nano Energy* **2019**, *56*, 840.
- [291] S. Li, L. Bai, N. Ji, S. Yu, S. Lin, N. Tian, H. Huang, *J. Mater. Chem. A* **2020**, *8*, 9268.
- [292] J. Wang, H. Yu, C. Hou, J. Zhang, *Sol. RRL* **2019**, *4*, 1900428.
- [293] B. Tang, L. Hou, M. Sun, F. Lv, J. Liao, W. Ji, Q. Chen, *Nanoscale* **2019**, *11*, 12817.
- [294] C. Xu, J. Mao, X. Guo, S. Yan, Y. Chen, T. W. Lo, C. Chen, D. Lei, X. Luo, J. Hao, C. Zheng, Y. Zhu, *Nat. Commun.* **2021**, *12*, 3665.
- [295] L. Liu, J. Dong, J. Huang, A. Nie, K. Zhai, J. Xiang, B. Wang, F. Wen, C. Mu, Z. Zhao, Y. Gong, Y. Tian, Z. Liu, *Chem. Mater.* **2019**, *31*, 10143.
- [296] M. Kupers, P. M. Konze, A. Meledin, J. Mayer, U. Englert, M. Wuttig, R. Dronskowski, *Inorg. Chem.* **2018**, *57*, 11775.
- [297] Y. Zhou, D. Wu, Y. Zhu, Y. Cho, Q. He, X. Yang, K. Herrera, Z. Chu, Y. Han, M. C. Downer, H. Peng, K. Lai, *Nano Lett.* **2017**, *17*, 5508.
- [298] Y. Li, M. Gong, H. Zeng, *J. Semicond.* **2019**, *40*, 061002.
- [299] M. Si, A. K. Saha, S. Gao, G. Qiu, J. Qin, Y. Duan, J. Jian, C. Niu, H. Wang, W. Wu, S. K. Gupta, P. D. Ye, *Nat. Electron.* **2019**, *2*, 580.
- [300] S. Wang, L. Liu, L. Gan, H. Chen, X. Hou, Y. Ding, S. Ma, D. W. Zhang, P. Zhou, *Nat. Commun.* **2021**, *12*, 53.
- [301] W. Ding, J. Zhu, Z. Wang, Y. Gao, D. Xiao, Y. Gu, Z. Zhang, W. Zhu, *Nat. Commun.* **2017**, *8*, 14956.
- [302] C. Cui, W. J. Hu, X. Yan, C. Addiego, W. Gao, Y. Wang, Z. Wang, L. Li, Y. Cheng, P. Li, X. Zhang, H. N. Alshareef, T. Wu, W. Zhu, X. Pan, L. J. Li, *Nano Lett.* **2018**, *18*, 1253.
- [303] F. Xue, W. Hu, K. C. Lee, L. S. Lu, J. Zhang, H. L. Tang, A. Han, W. T. Hsu, S. Tu, W. H. Chang, C. H. Lien, J. H. He, Z. Zhang, L. J. Li, X. Zhang, *Adv. Funct. Mater.* **2018**, *28*, 1803738.
- [304] J. Low, J. Yu, W. Ho, *J. Phys. Chem. Lett.* **2015**, *6*, 4244.
- [305] G. Gao, Y. Jiao, E. R. Waclawik, A. Du, *J. Am. Chem. Soc.* **2016**, *138*, 6292.
- [306] L. Ju, X. Tan, X. Mao, Y. Gu, S. Smith, A. Du, Z. Chen, C. Chen, L. Kou, *Nat. Commun.* **2021**, *12*, 5128.
- [307] M. C. O. Monteiro, F. Dattila, B. Hagedoorn, R. García-Muelas, N. López, M. T. M. Koper, *Nat. Catal.* **2021**, *4*, 654.
- [308] A. M. Leguy, J. M. Frost, A. P. McMahon, V. G. Sakai, W. Kochelmann, C. Law, X. Li, F. Foglia, A. Walsh, B. C. O'Regan, J. Nelson, J. T. Cabral, P. R. Barnes, *Nat. Commun.* **2015**, *6*, 7124.
- [309] S. Meloni, T. Moehl, W. Tress, M. Franckevicius, M. Saliba, Y. H. Lee, P. Gao, M. K. Nazeeruddin, S. M. Zakeeruddin, U. Rothlisberger, M. Graetzel, *Nat. Commun.* **2016**, *7*, 10334.
- [310] X. Zheng, B. Chen, J. Dai, Y. Fang, Y. Bai, Y. Lin, H. Wei, Xiao C. Zeng, J. Huang, *Nat. Energy* **2017**, *2*, 17102.
- [311] X. C. Ren, X. Q. Zhang, R. Xu, J. Q. Huang, Q. Zhang, *Adv. Mater.* **2020**, *32*, 1908293.
- [312] N. Kumar, S. N. Guin, K. Manna, C. Shekhar, C. Felser, *Chem. Rev.* **2021**, *121*, 2780.
- [313] X. Wang, K. Yasuda, Y. Zhang, S. Liu, K. Watanabe, T. Taniguchi, J. Hone, L. Fu, P. Jarillo-Herrero, *Nat. Nanotechnol.* **2022**, *367*, <https://doi.org/10.1038/s41565-021-01059-z>.
- [314] D. Bennett, B. Remez, *npj 2D Mater. Appl.* **2022**, *6*, 7.
- [315] J. Sung, C. Shin, *Micromachines* **2020**, *11*, 1125.
- [316] C. Zhan, T. Wu, J. Lu, K. Amine, *Energy Environ. Sci.* **2018**, *11*, 243.
- [317] Y. Zhang, P. Wang, T. Zheng, D. Li, G. Li, Y. Yue, *Nano Energy* **2018**, *49*, 596.
- [318] W. Li, J. Shi, K. H. L. Zhang, J. L. MacManus-Driscoll, *Mater. Horiz.* **2020**, *7*, 2832.
- [319] F. Yang, M. Li, L. Li, P. Wu, E. Pradal-Velázquez, D. C. Sinclair, *J. Mater. Chem. A* **2018**, *6*, 5243.



Xian-Kui Wei is a staff scientist at Ernst Ruska-Centre (ER-C) for Microscopy and Spectroscopy with Electrons in Forschungszentrum Jülich, Germany. After receiving his Ph.D. degree from Institute of Physics, Chinese Academy of Sciences in 2011, he worked as a collaborator scientist/postdoc in Swiss Federal Institute of Technology Lausanne (EPFL) until 2016. His research interest focuses on atomic-scale light-element imaging and polar ultramicroscopy structure of ferroelectric oxides, catalysts, batteries, topological insulators as well as structure–property relationship.



Neus Domingo has been CSIC Distinguished Researcher at the Catalan Institute of Nanoscience and Nanotechnology (ICN2) in Bellaterra (Spain), where she led the Advanced Atomic Force Microscopy Platform from 2016 to 2021, focusing her research on the physical chemistry of ferroelectric and polar surfaces. She received the Ph.D. degree from the Fundamental Physics Department of the University of Barcelona in 2005, and after a postdoctoral fellowship at the CNR in Italy and several research positions at CIN2 and ICN2 in Spain, she just joined the Oak Ridge National Laboratory (USA) in January 2022, where she is now the group leader of the Functional Atomic Force Microscopy group of the CNMS.



Young Sun is a full professor at the Center of Quantum Materials and Devices and the Department of Applied Physics in Chongqing University, People's Republic of China. He received Ph.D. degree in the Department of Physics, University of Science and Technology of China in 2001. After a postdoctoral research associate in University of Illinois at Urbana-Champaign and Rice University, he joined the Institute of Physics, Chinese Academy of Sciences in 2004 and moved to Chongqing University in 2021. His research interests focus on the physics and applications of multiferroic materials and magnetoelectric effects.



Nina Balke is an associate professor in the Materials Science and Engineering Department and the Director of the Analytical Instrumentation Facility at North Carolina State University (USA). She received her Ph.D. in Materials Science from the Technological University in Darmstadt Germany in 2006. Her research interest focuses on nanoscale materials' functionality driven by electric fields for information and energy technology. This includes the study of electromechanical, mechanical and transport phenomena in inorganic materials and across fluid-solid interfaces.



Rafal E. Dunin-Borkowski is Director of the Ernst RuskaCentre for Microscopy and Spectroscopy with Electrons (ER-C) and Institute for Microstructure Research (PGI-5) in Forschungszentrum Jülich and professor of Experimental Physics in RWTH Aachen University. His research involves the development of quantitative techniques in electron microscopy and has recently focused on the use of electron holography to study electromagnetic fields in nanoscale materials, thin films and devices. In 2009 he was awarded the Ernst Ruska Prize of the German Society for Electron Microscopy. In 2012 he was awarded an Advanced Grant by the European Research Council.



Joachim Mayer received his Ph.D. in Physics at the Max-Planck-Institut für Metallforschung, Stuttgart, Germany. In 1988 he joined the Materials Department at the University of California, Santa Barbara, as a postdoctoral research associate. In 1990 he moved back to the Max-Planck-Institut für Metallforschung, Stuttgart, where he worked as a research scientist and Group Leader “Analytical Electron Microscopy.” In 1999 he joined RWTH Aachen University to become professor and Head of the Central Facility for Electron Microscopy of RWTH Aachen. In 2004, he received a co-appointment as one of the two directors of the Ernst Ruska-Centre at Research Centre Juelich.